AWARD NUMBER: W81XWH-14-1-0429

TITLE: Understanding the Role of MDSCs in Castration-Resistant Prostate Cancer and Metastasis

PRINCIPAL INVESTIGATOR: Dr. Prasenjit Dey, Ph.D.

CONTRACTING ORGANIZATION: The University of Texas MD Anderson Cancer Center
Houston, TX 77030

REPORT DATE: December 2016

TYPE OF REPORT: Final

PREPARED FOR: U.S. Army Medical Research and Materiel Command
Fort Detrick, Maryland 21702-5012

DISTRIBUTION STATEMENT: Approved for Public Release; Distribution Unlimited

REPORT DOCUMENTATION PAGE

Form Approved
OMB No. 0704-0188

1. REPORT DATE December 2016	**2. REPORT TYPE** Final	**3. DATES COVERED** 15 Sep 2014 - 14 Sep 2016

4. TITLE AND SUBTITLE

Understanding the Role of MDSCs in Castration-Resistant Prostate Cancer and Metastasis

5a. CONTRACT NUMBER

5b. GRANT NUMBER
W81XWH-14-1-0429

5c. PROGRAM ELEMENT NUMBER

6. AUTHOR(S)

Prasenjit Dey, Ph.D.

E-Mail: pdey@mdanderson.org

5d. PROJECT NUMBER

5e. TASK NUMBER

5f. WORK UNIT NUMBER

7. PERFORMING ORGANIZATION NAME(S) AND ADDRESS(ES)

The University of Texas MD
Anderson Cancer Center
1515 Holcombe Boulevard
Houston, TX 77030-4009

8. PERFORMING ORGANIZATION REPORT NUMBER

9. SPONSORING / MONITORING AGENCY NAME(S) AND ADDRESS(ES)

U.S. Army Medical Research and Materiel Command
Fort Detrick, Maryland 21702-5012

10. SPONSOR/MONITOR'S ACRONYM(S)

11. SPONSOR/MONITOR'S REPORT NUMBER(S)

12. DISTRIBUTION / AVAILABILITY STATEMENT

Approved for Public Release; Distribution Unlimited

13. SUPPLEMENTARY NOTES

14. ABSTRACT

The androgen receptor is a primary target of prostate cancer treatment and prevention. For metastatic prostate cancer (androgen responsive), androgen deprivation therapy (ADT) has been the standard mode of treatment. The tumors initially respond with the inhibition of growth, but most tumors invariably relapse leading to a lethal castration resistant prostate cancer (CRPC), indicating a shift in tumor responsiveness. The proliferating primary tumor recruits a variety of stromal cells in its surrounding microenvironment, which facilitates its growth and ultimately invasion and metastasis to distant organs. The myeloid derived suppressor cells (MDSC) and regulatory T cells (Treg) are important components of the immune suppressive network of the tumor microenvironment (TMEN). MDSCs play a pivotal role in suppression of both innate and adaptive immunity and its presence is documented both in preclinical model and cancer patients. The role of MDSCs in prostate cancer CRPC and metastasis is poorly understood. The unanswered questions include how MDSCs facilitate the tumor cells to evade the host immune surveillance, and what pathway regulates MDSC recruitment, accumulation, proliferation and differentiation in prostate cancer. Using the PB-Cre4/$PTEN^{L/L}$/$SMAD4^{L/L}$ and PB-Cre4/$PTEN^{L/L}$/$Trp53^{L/L}$/ $SMAD4^{L/L}$ mouse model this project will first characterize MDSC population in both primary tumors as well as castration resistant tumors. Then we will identify novel prostate cancer specific MDSC markers using genomic and proteomic technology and finally, we will propose pre-clinical model to validate our newly discovered targets to deplete MDSCs to prevent/treat CRPC.

15. SUBJECT TERMS

16. SECURITY CLASSIFICATION OF:			**17. LIMITATION OF ABSTRACT**	**18. NUMBER OF PAGES**	**19a. NAME OF RESPONSIBLE PERSON** USAMRMC
a. REPORT Unclassified	**b. ABSTRACT** Unclassified	**c. THIS PAGE** Unclassified	Unclassified	35	**19b. TELEPHONE NUMBER** *(include area code)*

Standard Form 298 (Rev. 8-98)
Prescribed by ANSI Std. Z39.18

Table of Contents

Pages

1. INTRODUCTION:

The androgen receptor is a primary target of prostate cancer (PCa) treatment and prevention [1]. For metastatic prostate cancer, androgen deprivation therapy (ADT) has been the standard mode of treatment [2]. The tumors initially respond with the inhibition of growth, but most tumors invariably relapse leading to a lethal castration resistant prostate cancer (CRPC). The primary tumors recruit a variety of stromal cells in its surrounding microenvironment, which facilitates its growth and ultimately invasion and metastasis to distant organs [3]. The myeloid derived suppressor cells (MDSC) and regulatory T (Treg) cells are important components of the immune suppressive network of the tumor microenvironment (TMEN) [3-5]. They are a heterogeneous subset of activated but immature myeloid cells (IMC) [6]. In mice, MDSCs co-express myeloid cell lineage marker Gr-1^{mid} and CD11b^{hi} [7] and comprise two main subsets--monocytic (Ly6C^{hi}) and granulocytic (Ly6G^{hi}). It is well established that MDSCs suppress both innate and adaptive immunity and their presence in tumors is documented in both preclinical models and cancer patients [8]. However, the role of MDSCs in prostate cancer development is poorly understood. Recent data suggests that ADT promotes immune cells infiltration, which influences tumor relapse and resistance to castration [9, 10]. These immune cells cause inflammatory response leading to further infiltration and expansion of MDSCs into the tumor microenvironment making the tumor increasingly resistant to conventional chemotherapy and radiation-therapy [11, 12]. Given castration causes increase in the immune cell infiltration, we hypothesize that inflammation signal post-castration may lead to activation and further expansion of MDSCs within TMEN which may contribute to the development of CRPC. Given our preliminary data indicating the presence of large number of MDSCs in primary prostate tumors and depletion of MDSCs by neutralizing antibodies against Gr-1 leads to regression of primary tumor in our animal model, we further hypothesize that depletion of MDSCs would have therapeutic benefit for prostate cancer patients. We first characterized MDSC population in both primary tumors as well as castration resistant tumors as described in specific aim 1. Then we identified novel prostate cancer specific MDSC markers using genomic and proteomic technology in specific aim 2. Finally, in specific aim 3, we propose to validate our newly discovered targets to deplete MDSCs to prevent/treat CRPC.

2. **KEYWORDS:** Castration resistant prostate cancer (CRPC), tumor microenvironment (TMEN), androgen deprivation therapy (ADT), myeloid cells

3. ACCOMPLISHMENTS:

What were the major goals of the project?

Goal 1. Characterization of the prostate cancer mouse model to study MDSCs in CRPC and metastasis.

Goal 2. Identification of the novel genetic pathways in prostate cancer specific MDSCs by transcriptomic and proteomic analysis.

Goal 3. Functional validation of the role of MDSC in tumor progression and metastasis.

What was accomplished under these goals?

Aim 1. Characterization of MDSCs using the novel $Pten^{pc-/-}Smad4^{pc-/-}$ model. The goal for this specific aim is to further characterize this novel $Pten^{pc-/-}Smad4^{pc-/-}$ model we recently generated and to establish a cohort bearing primary, metastatic and castration resistant tumors for MDSC characterization.

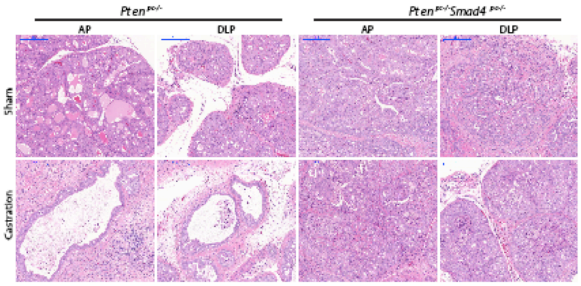

Figure 1: H & E staining of tumors from sham control and castrated mice ($Pten^{pc-/-}Smad4^{pc-/-}$ and $Pten^{pc-/-}$ mice) at 1 month post-ADT.

Current objective: **(a) Characterization of mice cohort to study MDSC in CRPC.** We have earlier reported castration in a larger cohort of mice and generated cumulative survival curve for this cohort (Data reported earlier). To further characterize our $Pten^{pc-/-}Smad4^{pc-/-}$ mutant mouse model we have now conducted surgical castration alone or in combination with Enzalutamide in $Pten^{pc-/-}Smad4^{pc-/-}$ mutant mice and assessed the affect on tumor response. We collected prostate tissues and non-prostate tissue from major organs such as bone, lung, and lymph nodes from these mice. In addition, lung and bone tissues from $Pten^{pc-/-};Smad4^{pc-/-}$ mutant mice with lethal CRPC and examined for increased lung metastasis and bone metastasis.

Methodology: Wild type, $Pten^{pc-/-}$ and $Pten^{pc-/-};Smad4^{pc-/-}$ mice are subjected to surgical castration or in combination with Enzalutamide treatment (10 mg/kg daily oral gavage). We collected tumors, draining lymph node and lungs after animals developed castration resistance and from animals bearing castration naïve tumors. At least five samples per group of spontaneous prostate tumors and those regrow after castration as well as regional lymph nodes and distant organs, were collected at 15 and 90 days post castration for detailed histopathological analyses (Figure 2).

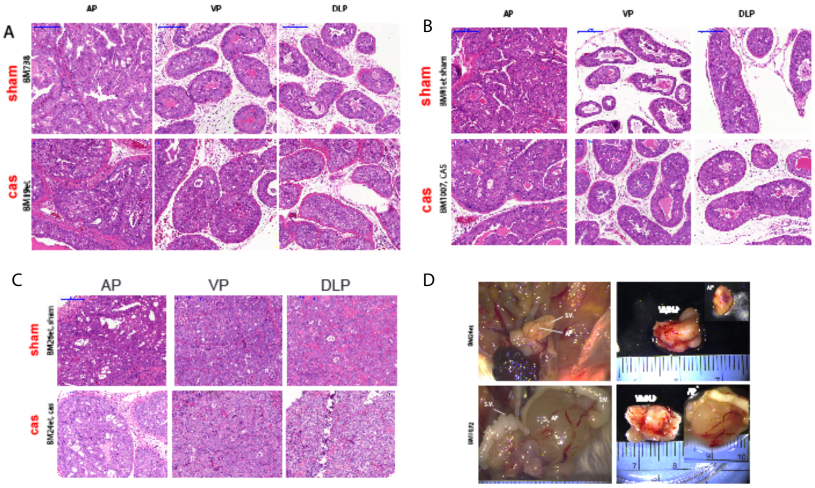

Figure 2: In $Pten^{pc-/-}Smad4^{pc-/-}$ tumors are resistance to Enzalutamide. (A) 2 weeks, (B) 4 weeks, and (C-D) 12 weeks post-castration+ Enzalutamide treatment.

Results:

1. *Pten*$^{pc-/-}$*Smad4*$^{pc-/-}$ tumors are resistant to surgical castration plus Enzalutamide. We performed surgical castration alone or in combination with Enzalutamide treatment in *Pten*$^{pc-/-}$*Smad4*$^{pc-/-}$ and *Pten*$^{pc-/-}$ mice. Tumors were harvested at 2, 4, 8, and 12 weeks post-ADT and subjected to histopathological analysis. In consistent with previous report [13, 14], *Pten*$^{pc-/-}$ tumors are sensitive to ADT. A significant amount of normal epithelium was identified in castrated *Pten*$^{pc-/-}$ mice at 1 and 2 months post-castration, suggesting a clear response to castration (Fig. 1). On the contrary, *Pten*$^{pc-/-}$*Smad4*$^{pc-/-}$ mice are resistant to castration as compared to *Pten*$^{pc-/-}$ as shown by histopathological analysis by H & E staining (Fig. 2A-D) and MRI analysis (data not shown). There is no noticeable normal epithelium in the castrated *Pten*$^{pc-/-}$*Smad4*$^{pc-/-}$ mice 1, 2, and 3 months post-castration, suggesting loss of *Smad4* in a *Pten*-null genetic context confers a *de novo* resistance to ADT.

(b) Characterization of MDSCs and other immune cell populations in naïve vs. castrated tumor. We characterized the MDSC in a large cohort of mice using the well-established markers such as CD11b$^+$Gr-1$^+$ MDSCs in stroma.

Methodology: To obtain a dynamic view of infiltrating immune cells as a function of tumor progression in the *Pten*$^{pc-/-}$*Smad4*$^{pc-/-}$ mouse model, we performed mass cytometry (CyTOF) immunophenotyping of 17 surface markers [15] to catalog tumor cell type constituents from well-established tumors in 16-week old *Pten*$^{pc-/-}$ and *Pten*$^{pc-/-}$*Smad4*$^{pc-/-}$ mice.

Results: 1. Increase infiltration of CD11b+Gr1+ MDSC cells into the tumor. CyTOF confirmed a significant increase of CD45$^+$ infiltrating leukocytes in *Pten*$^{pc-/-}$*Smad4*$^{pc-/-}$ as compared to *Pten*$^{pc-/-}$ tumors. Within the CD45$^+$ infiltrating cells, CD11b$^+$ myeloid cells represent a remarkably increased population in *Pten*$^{pc-/-}$*Smad4*$^{pc-/-}$ as compared to *Pten*$^{pc-/-}$ tumors (Fig. 3).

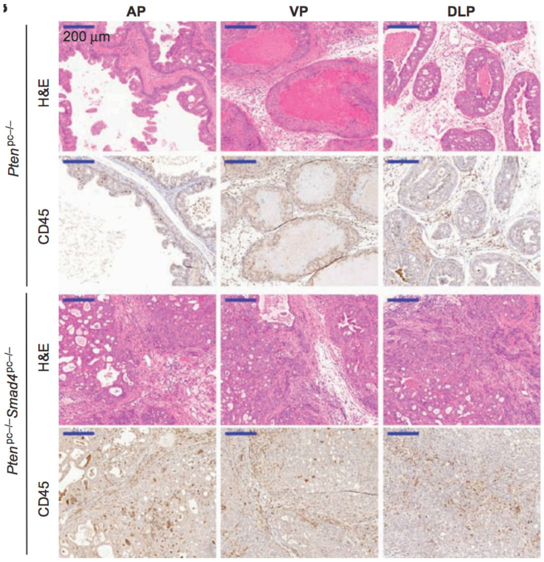

Figure 3: Increase in the infiltration of immune cells as shown by IHC for CD45 in *Pten*$^{pc-/-}$*Smad4*$^{pc-/-}$ tumors as compared with Ptenpc−/− tumors from 16-week-old mice (n = 3). AP, anterior prostate; VP, ventral prostate; DLP, dorsolateral prostate; H&E, hematoxylin and eosin staining. Scale bars, 200 µm.

The detailed immunophenotyping profiles enabled construction of the spanning-tree progression analysis of density-normalized events (SPADE)–derived tree. SPADE is a computational approach to facilitate the identification and analysis of heterogeneous cell types. SPADE of the *Pten*$^{pc-/-}$*Smad4*$^{pc-/-}$ model displays the complexity of the TME, which is composed of epithelial tumor cells (EpCAM+CD45−), nonimmune TME cells (EpCAM−CD45−), and infiltrating immune cells (EpCAM−CD45+) that can be further grouped into various immune cell subpopulations (Fig. 4A). Among the infiltrating immune cells, there was a striking age-dependent increase of CD11b+Gr1+ cells in tumors (Fig. 4B); this trend was much less pronounced in the spleen or draining lymph nodes (Data not shown).

2. MDSCs are highly immunosuppressive. To evaluate the potential immunosuppressive activity of intratumoral CD11b+Gr1+ cells from *Pten*$^{pc-/-}$*Smad4*$^{pc-/-}$ tumors, we examined T-cell proliferation using a standard T cell suppression assay. The CD11b+Gr1+ cells strongly suppressed CD3 and

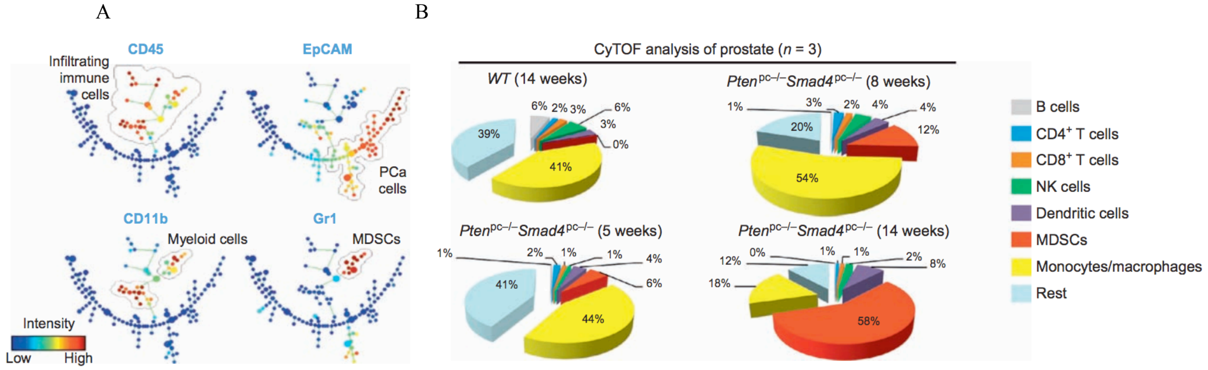

Figure 4: A, SPADE tree derived from CyTOF (17-marker) analysis of whole-tumor cell population from Ptenpc−/−Smad4pc−/− mice at 5 weeks, 8 weeks, and 14 weeks of age (n = 3). Live single cells were used to construct the tree. Cell populations were identified as prostate cancer (PCa) cells (EpCAM+CD45−), nonimmune TME cells (EpCAM−CD45−), T cells (CD45+CD3+TCRβ+), B cells (CD45+B220+CD19+), natural killer (NK) cells (CD45+NK1.1+), dendritic cells (CD45+CD11c+), putative MDSCs (CD45+CD11b+Gr1+), and macrophages (CD45+CD11b+Gr1−). On the right plots, the tree is colored by the median intensity of individual markers shown on the top to highlight infiltrating immune cells (EpCAM−CD45+), epithelial prostate cancer cells (EpCAM+CD45−), total myeloid cells (CD45+CD11b+), and putative MDSCs (CD45+CD11b+Gr1+). B, CyTOF analysis of tumors from 5-, 8-, and 14-week-old Ptenpc−/−Smad4pc−/− mice revealed an age-dependent increase in the MDSC infiltration. Prostate from wild-type (WT) mice at 16 weeks old was used as control (n = 3 for each genotype).

CD28 antibody-induced T-cell proliferation and activation (Fig. 5A), establishing that CD11b+Gr1+ cells are indeed functional MDSCs. MDSCs can be further classified as a $\text{Ly6G}^{+}\text{Ly6C}^{lo}$ subset with polymorphonuclear phenotype (PMN-MDSC) and a $\text{Ly6G}^{-}\text{Ly6C}^{hi}$ subset with monocytic phenotype (M-MDSC). PMN-MDSCs represented the major MDSC population in *Pten*$^{pc-/-}$*Smad4*$^{pc-/-}$ tumors (See attached appendix), consistent with previously observed preferential expansion of PMN-MDSCs in tumor-bearing mice of various syngeneic models [16, 17]. The abundance of PMN-MDSCs was further

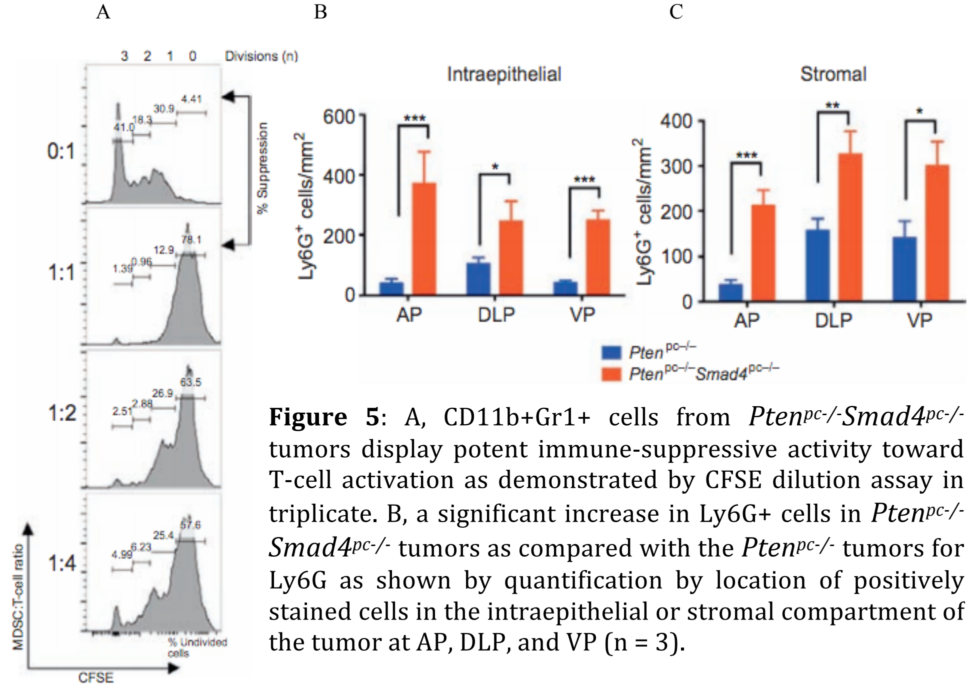

Figure 5: A, CD11b+Gr1+ cells from *Pten*$^{pc-/-}$*Smad4*$^{pc-/-}$ tumors display potent immune-suppressive activity toward T-cell activation as demonstrated by CFSE dilution assay in triplicate. B, a significant increase in Ly6G+ cells in *Pten*$^{pc-/-}$*Smad4*$^{pc-/-}$ tumors as compared with the *Pten*$^{pc-/-}$ tumors for Ly6G as shown by quantification by location of positively stained cells in the intraepithelial or stromal compartment of the tumor at AP, DLP, and VP (n = 3).

confirmed by IHC for Ly6G, as shown by quantification of both intraepithelial and stromal Ly6G+ cells in tumors from *Pten*$^{pc-/-}$*Smad4*$^{pc-/-}$ mice and *Pten*$^{pc-/-}$ mice (Fig. 5B). It has been shown previously that ROS production by PMN-MDSCs is one of the mechanisms driving immune suppression [18, 19]. Correspondingly, IPA revealed that pathways involved in ROS and nitric oxide (NO) production are among the top pathways activated in *Pten*$^{pc-/-}$*Smad4*$^{pc-/-}$ tumors (See attached appendix). Consistent with the increased infiltration of PMN-MDSCs in the *Pten*$^{pc-/-}$*Smad4*$^{pc-/-}$ tumors, the expression of several subunits of NADPH oxidase (Nox2, p40phox, and p47phox), which are responsible for ROS production in PMN-MDSCs, was significantly upregulated in *Pten*$^{pc-/-}$*Smad4*$^{pc-/-}$ tumors relative to *Pten*$^{pc-/-}$ tumors (See attached appendix). Moreover, Arg1, but not Nos2, was highly upregulated in the *Pten*$^{pc-/-}$*Smad4*$^{pc-/-}$ tumors (See attached appendix). Together, MDSCs in autochthonous *Pten*$^{pc-/-}$*Smad4*$^{pc-/-}$ tumors display strong T-cell–suppressive activity and are predominantly the PMN-MDSC subtype.

Aim 2. Identification of the novel genetic pathways in prostate cancer specific MDSCs by transcriptomic and proteomic analysis. The goal of this aim is to utilize powerful genomic profiling technologies to identify novel genes and pathways that drive the development of CRPC.

Current objective: We have observed a unique role of Smad4 in CRPC where conditional deletion of Smad4 bypassed the senescence barrier instigated by Pten loss in the prostate epithelia, resulting in a highly proliferative and invasive prostate adenocarcinoma characterized by an exuberant stromal reaction and frequent metastasis to distant organs. To understand the biology behind castration resistance observed upon Smad4 deletion we compared the *Pten*$^{pc-/-}$ and *Pten*$^{pc-/-}$*Smad4*$^{pc-/-}$ mouse model.

Methodology: To enable unambiguous distinction between tumor and stroma, we incorporated a dual fluorescent reporter allele, Rosa26-Lox-tdTomato-Lox-EGFP (a.k.a. mTmG), into the PB-Cre+ *Pten*$^{pc-/-}$*Smad4*$^{pc-/-}$ model. This allele allows Cre-dependent GFP expression in prostate epithelial cells as well as ubiquitous tdTomato expression in all other cells (Figure 6). We now can (1) visualize tumor and stroma distinctly by fluorescence imaging, (2) visually quantify metastases in lymph node and lung without laborious histological inspection, and (3) easily isolate tumor and stromal cells using flow cytometry or Laser Capture Microdissection. Furthermore, to enable noninvasive bioluminescence imaging (BLI) of tumor and metastasis development, we have further incorporated Rosa26-Lox-STOP-Lox-Luciferase allele and have confirmed the prostate-specific luciferase signal (Figure 6). Thus, we now have established a robust metastatic PCa model: PB-Cre^{+} *Pten*$^{pc-/-}$*Smad4*$^{pc-/-}$ *mTmG*$^{L/+}$*Luc*$^{L/+}$, which will facilitate monitoring of tumor development and tumor-stroma interactions through dual fluorescence and bioluminescence imaging. In parallel, we have also established a comparable model with only Pten loss: PB-Cre^{+} Pten$^{L/L}$ mTmG$^{L/+}$ Luc$^{L/+}$. It is

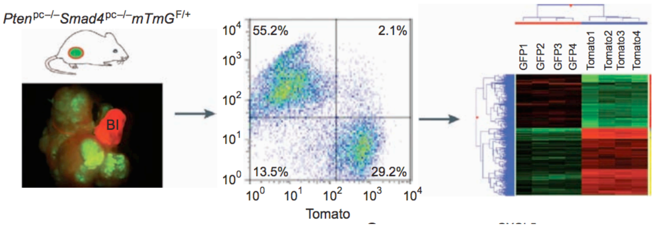

Figure 6: Establishment of *Pten*$^{pc-/-}$*Smad4*$^{pc-/-}$ model allows fluorescent visualization of the GFP+ tumor cells intermixed with Tomato+ stroma (left; FACS isolation of GFP+ tumor cells and Tomato+ stromal cells from the prostate adenocarcinoma (middle); microarray analysis to identify differentially expressed genes (right). In the fluorescence image, Bl denotes bladder (completely Tomato+; n = 2).

important to note that we have now backcrossed these strains to C57BL/6 congenic background, which enables syngeneic transplantation.

Results:

1. Transcriptomic profiling of GFP+ tumor cells and Tomato+ stromal cells from *Pten*$^{pc-/-}$*Smad4*$^{pc-/-}$ shows a distinct expression pattern for these two populations. We isolated GFP+ tumor cells and Tomato+ stromal cells, from which RNAs were isolated and subjected to microarray analysis. As expected, tumor and stroma showed distinct expression pattern by Hierachical Clustering Analysis (See attached appendix), and IPA indicated that while tumor cells are enriched for pathways involving cell adhesion molecules and tight junction (consistent with their epithelial nature), stromal cells display activation of more diverse signaling pathways involved in chronic inflammation, such as cytokine/cytokine receptor interaction, chemokine signaling pathway, Jak-STAT pathway, TCR pathway, and BCR pathway ($p<0.01$, data not shown).

2. CXCL5–CXCR2 Signaling Promotes MDSC Recruitment and CXCR2 Inhibition Delays Tumor Progression in *Pten*$^{pc-/-}$*Smad4*$^{pc-/-}$ mice. Employing this novel model, we sought to identify genes that were upregulated in *Pten*$^{pc-/-}$*Smad4*$^{pc-/-}$ cancer cells relative to *Pten*$^{pc-/-}$ cancer cells that might illuminate mechanisms involved in the recruitment of MDSCs by classifying the upregulated genes into either stroma- or tumor-enriched genes. To this end, our previously generated list of 242 genes with greater than 2-fold increased expression in *Pten*$^{pc-/-}$*Smad4*$^{pc-/-}$ relative to *Pten*$^{pc-/-}$ tumors [20] was intersected with 486 genes preferentially expressed in *Pten*$^{pc-/-}$*Smad4*$^{pc-/-}$*GFP+* cancer cells relative to Tomato+ stroma cells (fold change ≥4), yielding 28 genes that are markedly enriched in *Pten*$^{pc-/-}$*Smad4*$^{pc-/-}$ cancer cells. Among these 28 genes, Cxcl5, which encodes a key cytokine involved in MDSC recruitment [21], is the most significantly upregulated cancer cell–specific cytokine in *Pten*$^{pc-/-}$*Smad4*$^{pc-/-}$ tumors as compared with *Pten*$^{pc-/-}$ tumors (Fig. 7A).

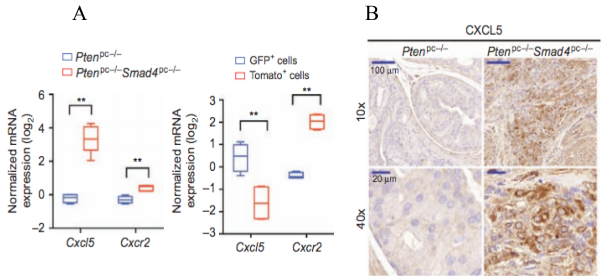

Figure 7: Quantification of mRNA expression shows that Cxcl5 and Cxcr2 were both expressed at higher levels in *Pten*$^{pc-/-}$*Smad4*$^{pc-/-}$ tumors than in *Pten*$^{pc-/-}$ tumors, and Cxcl5 expression was enriched in GFP+ tumor cells, whereas Cxcr2 expression was enriched in Tomato+ stromal cells (n = 5). C, IHC for CXCL5 showed significantly higher expression levels of CXCL5 in *Pten*$^{pc-/-}$*Smad4*$^{pc-/-}$ tumors than *Pten*$^{pc-/-}$ tumors (n = 3).

Notably, CXCR2, the cognate receptor for CXCL5, is also upregulated in *Pten*$^{pc-/-}$*Smad4*$^{pc-/-}$ tumors as compared with *Pten*$^{pc-/-}$ tumors and is significantly enriched in *Pten*$^{pc-/-}$*Smad4*$^{pc-/-}$ *Tomato+* stroma cells (Fig. 7A). The upregulation of CXCL5 expression in *Pten*$^{pc-/-}$*Smad4*$^{pc-/-}$ prostate tumors was further confirmed by IHC (Fig. 7b). In addition, we performed FACS analysis of CD11b+Gr1+ cells and CD11b−Gr1− cells from bone marrow, spleen, peripheral blood, and tumors for CXCR2 expression and found that CD11b−Gr1− cells (largely lymphocytes) are devoid of CXCR2 expression, whereas a large fraction of CD11b+Gr1+ cells express CXCR2. When CXCR2 expression was further separated into CXCR2^{hi} and CXCR2^{+}, we observed an enrichment of the CXCR2^{hi} subpopulation in the CD11b^{+}Gr1^{+} cells in prostate tumors (data not shown).

Aim 3: Functional validation of the role of MDSC in tumor progression and metastasis.

Current objective: To validate the CXCL5–CXCR2 axis in the recruitment of MDSCs to the TME of *Pten*$^{pc-/-}$*Smad4*$^{pc-/-}$ tumors, we assessed the impact of pharmacologic inhibition of CXCL5 and CXCR2 in MDSCs using a transwell migration assay.

Methodology: We used pharmacological approach to inhibit CXCL5 and CXCR2 followed by immunological and histopathological analysis of tumor to assess the infiltration of MDSCs.

Results:

1. CXCR2 inhibitor SB255002 or anti-CXCR2 neutralizing antibody pretreatment impeded migration of MDSCs. First, anti–CXCL5-neutralizing antibody pretreatment of conditioned medium (CM) derived from $Pten^{pc-/-}Smad4^{pc-/-}$ prostate cancer cell line resulted in decreased migration of MDSCs (See attached appendix). Second, CXCR2 inhibitor SB255002 or anti-CXCR2 neutralizing antibody pretreatment also impeded migration of MDSCs (Fig. 8A-B). Third, *in vivo* blockade of the CXCL5–CXCR2 axis using SB255002 in 14-week-old $Pten^{pc-/-}Smad4^{pc-/-}$ mice over a 14-day daily dosing schedule revealed a dramatic reduction in infiltration of MDSCs in the prostate tumors (See attached appendix). Notably, similar to mice treated with anti-Gr1 neutralizing antibody, these SB225002-treated $Pten^{pc-/-}Smad4^{pc-/-}$ mice also showed significant reduction in tumor burden (VP and DLP) as compared with the vehicle treated controls (Fig. 8C). Strikingly, all SB225002-treated

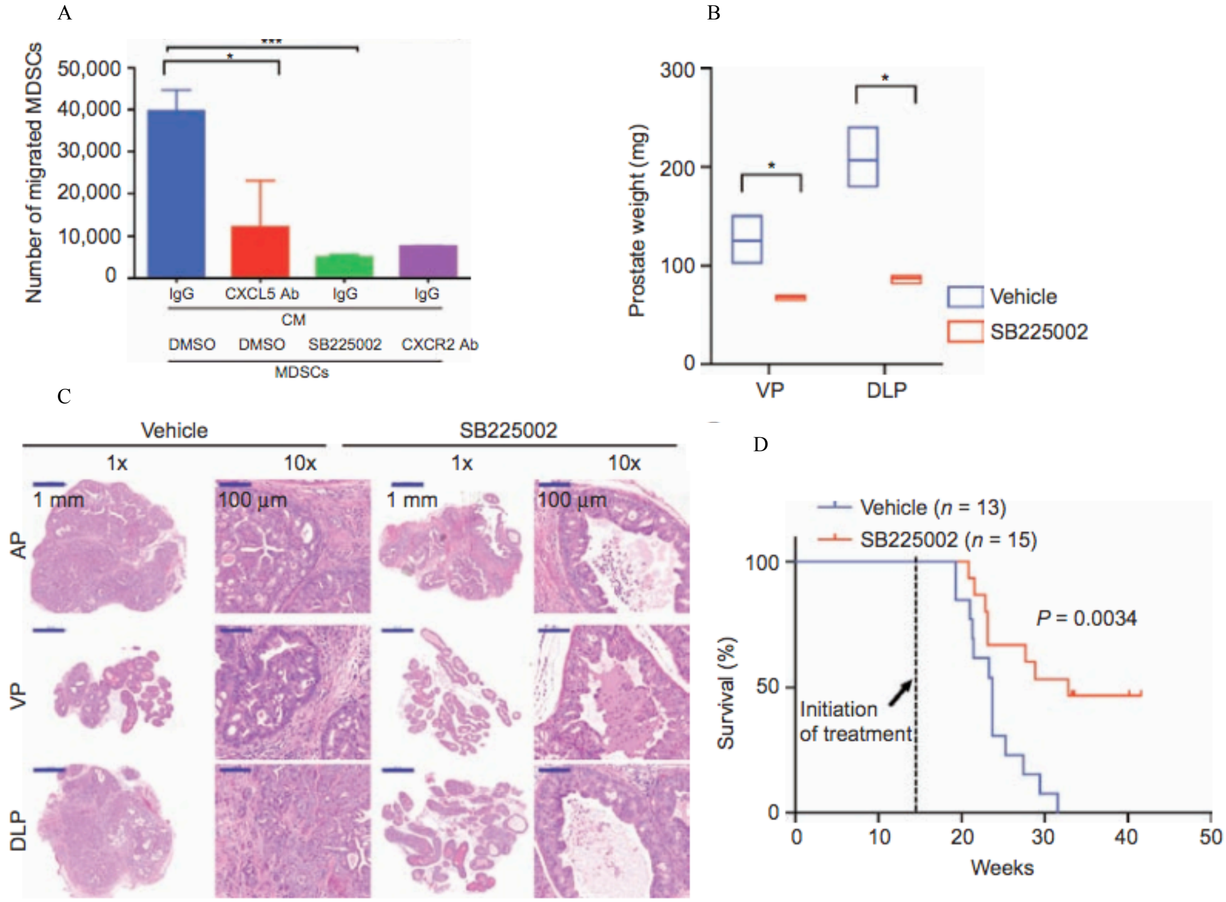

Figure 8: Blocking the CXCL5–CXCR2 axis by CXCL5-neutralizing antibody, CXCR2 inhibitor SB225002, or CXCR2-neutralizing antibody significantly decreased migration of MDSCs toward conditioned medium from $Pten^{pc-/-}Smad4^{pc-/-}$ tumor cells, evaluated with an in vitro transwell migration assay in triplicate. E and F, CXCR2 inhibitor SB225002 treatment of $Pten^{pc-/-}Smad4^{pc-/-}$ mice for 14 days (n = 4) resulted in significantly reduced tumor weight of VP and DLP and significantly delayed progression for AP prostate cancer shown by hematoxylin and eosin staining. G, CXCR2 inhibitor SB225002 treatment of $Pten^{pc-/-}Smad4^{pc-/-}$ mice significantly prolonged their overall survival.

tumors presented with prostatic intraepithelial neoplasia (PIN) pathology, whereas the control group uniformly possessed advanced adenocarcinoma (See attached appendix). Furthermore, SB225002 treatment significantly prolonged the overall survival of the *Pten*$^{pc-/-}$*Smad4*$^{pc-/-}$ mice as compared with the vehicle control (Fig. 8D). Thus, we conclude that the CXCL5–CXCR2 axis plays a prominent role in the recruitment of MDSCs to the *Pten*$^{pc-/-}$*Smad4*$^{pc-/-}$ prostate TME and that inhibition of this axis profoundly impairs tumor progression.

2. YAP1 is activated in *Pten*$^{pc-/-}$*Smad4*$^{pc-/-}$ tumors and directly regulates Cxcl5 transcription. Having identified cancer cell–derived CXCL5 as a key-signaling molecule governing recruitment of MDSCs into the TME, we sought to define the molecular mechanisms underlying the strong induction of CXCL5 expression in the *Pten*$^{pc-/-}$*Smad4*$^{pc-/-}$ cancer cells. As CXCL5 expression is not significantly upregulated in the *Pten*$^{pc-/-}$ tumors (See attached appendix), we performed unbiased Gene Set Enrichment Analysis (GSEA) to identify pathways that were activated in the *Pten*$^{pc-/-}$*Smad4*$^{pc-/-}$ tumors as compared with *Pten*$^{pc-/-}$ tumors, aiming to identify potential regulators for Cxcl5 in *Pten*$^{pc-/-}$*Smad4*$^{pc-/-}$ tumors. The YAP oncogenic signature emerged as the second most hyperactivated pathway (Fig. 9A). Although it is known that the Hippo–YAP pathway plays an important role in development and cancer in organs such as the liver, skin, intestine, and pancreas [22], the role for the Hippo–YAP pathway in prostate cancer biology is emerging. Specifically, Hippo pathway components LATS1/2 have been implicated in anoikis and metastasis in prostate cancer [23], and ERG-induced YAP1 activation can promote age-related prostate tumor development [24]. However, beyond the cancer cell–specific functions, the Hippo–YAP1 pathway has not been linked to signaling communication between cancer cells and immune cells in the TME. Consistent with the in silico analysis, IHC analysis documented a dramatic increase in the nuclear localization of YAP1 in *Pten*$^{pc-/-}$*Smad4*$^{pc-/-}$ cancer cells as compared with *Pten*$^{pc-/-}$ cancer cells (Fig. 9B). As YAP1, a transcriptional coactivator and the downstream mediator of Hippo signaling, is regulated post-transcriptionally by either kinase mediated degradation or cytoplasmic sequestration [22], our findings of increased nuclear localization of YAP1 are consistent with the hypothesis that the Hippo–YAP pathway is activated in the *Pten*$^{pc-/-}$*Smad4*$^{pc-/-}$ tumors. In addition, unbiased oPOSSUM analysis [25] indicated that TEAD1, a member of the TEAD transcription factor family that is

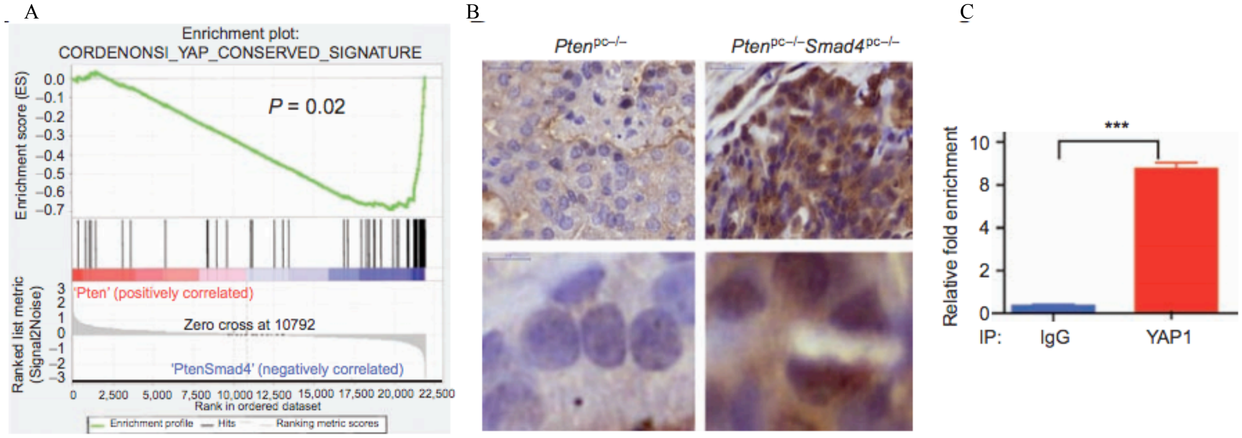

Figure 9: A, GSEA analysis identified the YAP1 oncogenic signature as the top activated pathway in the *Pten*$^{pc-/-}$*Smad4*$^{pc-/-}$ tumors compared with Ptenpc–/– tumors (n = 5). B, a significant increase in nuclear staining of YAP1 in the *Pten*$^{pc-/-}$*Smad4*$^{pc-/-}$ tumors compared with *Pten*$^{pc-/-}$ tumors (n = 3). C, ChIP shows that YAP1 can directly bind to Cxcl5 promoter using quantitative PCR in triplicates.

required for YAP1 function, ranked second among the top 10 transcription factors with overrepresented binding sites in the 70 cancer-specific genes that were upregulated in the $Pten^{pc-/-}$ $Smad4^{pc-/-}$ tumors as compared with the $Pten^{pc-/-}$ tumors (≥1.5 fold, Z-Score = 13.362; See attached appendix), an observation reinforcing the relevance of the Hippo–YAP pathway. Furthermore, we identified six YAP/TEAD binding motifs in the promoter of Cxcl5 gene (Supplementary Fig. S6D), suggesting YAP1 could be directly involved in the recruitment of MDSCs through regulating Cxcl5 expression. This hypothesis was supported by chromatin immunoprecipitation (ChIP) assay showing that YAP1 binds to Cxcl5 promoter (Fig. 9C) and that shRNA-mediated knockdown of Yap1 in $Pten^{pc-/-}Smad4^{pc-/-}$ cancer cells drastically reduced the expression of Cxcl5 mRNA (See attached appendix).

3. YAP1 Is Activated in Human Prostate Cancer and Tracks with an MDSC Signature. To determine whether YAP1 is overexpressed and activated in human prostate cancer, we performed IHC staining of a human prostate cancer tissue microarray (TMA) for YAP1. Interestingly, YAP1 is expressed in basal cells, but not in the luminal cells of the normal human prostate (See attached appendix). In addition, we observed that YAP1 is overexpressed in a subset of human prostate cancers (See attached appendix), consistent with a recent report [24]. Given the lack of validated antibodies for human MDSCs for TMA analysis, we generated a list of 39 MDSC-related genes curated from literature analysis (See attached appendix) to generate evidence of a link between YAP1 activation and MDSC prominence in human prostate. Using the prostate RNA-sequencing data from The Cancer Genome Atlas (TCGA), unsupervised clustering with the 39-gene MDSC signature categorized 498 TCGA primary prostate tumors into three subtypes: MDSC-high (n = 139), MDSC-medium (n = 158), and MDSC-low (n = 201; See attached appendix), suggesting that a subset of human prostate tumors may have prominent infiltration of MDSCs. In addition, using GSEA, we found that several YAP1 signature genes are significantly overexpressed in MDSC-high samples as compared with MDSC-low samples (See attached appendix; P value < 0.005), reinforcing the link between MDSC-high prostate tumors and YAP1 transcriptional activities.

Conclusion: The primary goal of this project is to elucidate the role played by castration in inflammation induced MDSC infiltration into tumor microenvironment. I have accomplished all the goals proposed for the project as stated in statement of works. I have generated all the cohorts necessary for the study and isolate tissues for further downstream analysis. I have also completed immunophenotyping by flow cytometry and CyTOF. I also have completed collection of samples for genomic/transcriptomic analysis by microarray and RNAseq and the data are now been analyzed by bioinformaticians. I have also identified a chemokine factor, CXCL5 that is responsible for MDSC infiltration and demonstrated that inhibition of CCR2 can be a therapeutic target in castrated resistant prostate cancer. I also have identified an upstream regulator of CXCL5, the transcriptional coactivator Yap1.

What opportunities for training and professional development has the project provided?

1) Training from intra- and inter-laboratory interactions: DePinho lab provides the best possible research environment. At MDACC, we have weekly lab meeting and journal club with post-doctoral fellow and graduate students from Ronald DePinho, Raghu Kalluri and Giulio Draetta's labs, which provide great opportunities to present my work in a critical academic setting and to learn about emerging discoveries from other talented post-docs and graduate students. At MDACC, I am exposed to a whole array of facilities and cores, whose core teams are willing to assist me in different aspects of my research. In addition, I have maintained a good relationship with bioinformaticians and biostatisticians led by Dr. Zhang and the scientists from the Institute of Applied Cancer Science led by Dr. Draetta. By collaborating and exchanging ideas with these scientists and physicians, I not only benefit from their great science, but will also build up a strong network for my future independent career.

2) Grant writing: With the help of Dr. DePinho, I successfully got the Department of Defense Prostate Cancer Research Program Postdoctoral Training Award. In addition, I'm helping Dr. DePinho to put together a CIPRIT MIRA grant and a RO1 grant on the role of MDSC using the novel prostate cancer mouse model generated in our lab. These experiences are invaluable, as Dr. DePinho will work closely with me to make sure I learn and understand the craft of grant writing. I also attended one workshops conducted by MDACC named "Write Winning Grants". These training activities will help me obtain funding for my independent research laboratory.

3) Scientific communication in writing: I'm working closely with Dr. DePinho in writing my research article on the novel molecular mechanisms for CRPC in the Pten/Smad4 mouse model along with Drs. Guocan Wang and Xin Lu. I expect to write another co-first-author papers on several novel mouse PCa models in collaboration projects with Dr. Xin Lu in our lab before I finish my postdoctoral training here. Furthermore, I attended the "Writing and Publishing Scientific Articles Workshop" in MDACC. These training experiences will help me to write and publish high-profile papers of my own laboratory.

4) Scientific communication in speaking: I routinely present my work in the DePinho lab meeting every other month in MDACC. I also regularly present my work in the joined weekly lab meeting among Draetta lab/Kalluri lab/DePinho lab/IACS and in the weekly Cancer Biology Department Seminar. In addition, I present regularly in the weekly Department of Cancer Biology Journal club. Moreover, I took the workshops provided by MDACC such as "Giving Presentations: Learn Presentation Skills and Tips That Will Help You Keep Your Audience Enthralled" and on similar topics. I believe these training activities will make presentation skill one of my strengths and help me interview for and attain a faculty position.

5) Lab management/Mentoring training: All of DePinho's postdoctoral fellows participate heavily in ensuring that various aspects of the lab are running smoothly. I have trained 1 undergraduate intern students, one medical intern student. These experiences have provided me the great opportunity to practice my mentoring and management skills. In terms of education for myself, I attended the "Faculty Mentoring Academy Series" at MDACC. Finally, I will continue to learn from Dr. DePinho, who is a master of mentoring himself, to improve a wide range of skills on mentoring and management.

6) Seminar series/Conferences/Workshops: MDACC offer a wide range of top-notch seminars/series/conferences, where I keep abreast of current research findings around the world. I also plan to attend various international conferences including but not limited to AACR Annual conference 2017 and SITC 2017. In addition to the workshops mentioned in other sections, I will attend "Faculty Development Workshop and Seminar Series" of MDACC regularly to help me prepare the transition to independent PI.

How were the results disseminated to communities of interest?

We have published our data in a highly competitive peer1   reviewed journal "Cancer Discovery" which has been received positively by the scientific community.

What do you plan to do during the next reporting period to accomplish the goals?

This is the final report and I have accomplished all the goals as proposed in the grant.

4. IMPACT:

What was the impact on the development of the principal discipline(s) of the project?

a. Comprehensive histopathological analysis of CRPC in the Pten/Smad4 mice suggests an expansion of the prostate tumor cells that express basal cell markers, such as Ck5 and p63. These basal type CRPC cells are highly proliferative, suggesting it may contain the cancer stem cell population.
b. Transcriptome profiling of GFP+ tumor cells and Tomato+ cells from Pten/Smad4/mTmG model identified tumor- and stroma-specific genes and pathways.
c. Integrative analysis of our published microarray dataset GSE25140 and the new Pten/Smad4 tumor/stroma dataset identified novel pathways that may play an important role in prostate cancer progression, metastasis, and resistance to ADT and resistance to MDV3100, such as Rb/E2Fs, AR, and Hippo/YAP1 pathways.
d. Identified a chemokine factor, CXCL5 that is responsible for MDSC infiltration.
e. Identified an upstream regulator of CXCL5, the transcriptional coactivator Yap1.

What was the impact on other disciplines?

Our recent publication in Cancer Discovery has the potential to translate into clinical trial to target CXCR2 using anti-CXCR2 therapy.

What was the impact on technology transfer?

"Nothing to Report."

What was the impact on society beyond science and technology?

"Nothing to Report."

CHANGES/PROBLEMS:

Changes in approach and reasons for change

"Nothing to Report."

Actual or anticipated problems or delays and actions or plans to resolve them

"Nothing to Report."

Changes that had a significant impact on expenditures

Describe changes during the reporting period that may have had a significant impact on expenditures, for example, delays in hiring staff or favorable developments that enable meeting objectives at less cost than anticipated.

Significant changes in use or care of human subjects, vertebrate animals, biohazards, and/or select agents

Describe significant deviations, unexpected outcomes, or changes in approved protocols for the use or care of human subjects, vertebrate animals, biohazards, and/or select agents during the reporting period. If required, were these changes approved by the applicable institution committee (or equivalent) and reported to the agency? Also specify the applicable Institutional Review Board/Institutional Animal Care and Use Committee approval dates.

Significant changes in use or care of human subjects

"Nothing to Report."

Significant changes in use or care of vertebrate animals.

"Nothing to Report."

Significant changes in use of biohazards and/or select agents

"Nothing to Report."

5. PRODUCTS:

Publications, conference papers, and presentations

Journal publications. *List peer-reviewed articles or papers appearing in scientific, technical, or professional journals. Identify for each publication: Author(s); title; journal; volume: year; page numbers; status of publication (published; accepted, awaiting publication; submitted, under review; other); acknowledgement of federal support (yes/no).*

1. Guocan Wang[1,2,*], Xin Lu[1,2*], **Prasenjit Dey**[1,2], Pingna Deng[1,2], Chia Chin Wu[4], Shan Jiang[2], Zhuangna Fang[2], Kun Zhao[2], Ramakrishna Konaparthi[2], Sujun Hua[1,2], Jianhua Zhang[4], Elsa M. Li Ning Tapia[5], Avnish Kapoor[2], Chang-Jiun Wu[4], Neelay Bhaskar Patel[2], Zhenglin Guo[1,2], Vandhana Ramamoorthy[4], Trang N. Tieu[4], Tim Heffernan[4], Di Zhao[1,2], Xiaoying Shang[1], Sunada Khadka[1], Pingping Hou[1,2], Baoli Hu[1,2], Xiaolu Pan[2], Zhihu Ding[3], Yanxia Shi[2], Liren Li[2], Edward Chang[4], Patricia Troncoso[6], Christopher J. Logothetis[5], Mark McArthur[7], Lynda Chin[2], Y. Alan Wang[1,2], Ronald A. DePinho[1]. Targeting YAP-dependent MDSC infiltration impairs tumor progression. *Cancer Discover* 2016 Jan; 6(1): 80–95.

DOD grant (W81XWH-14-1-0429) has been acknowledged in the publication.

- **Books or other non-periodical, one-time publications.**

"Nothing to Report."

Other publications, conference papers, and presentations.

1. Di Zhao, Xin Lu, Guocan Wang, Zangdao Lan, Wen-Ting Liao, Jun Li, Xin Liang, Jasper Chen, Sagar Shah, Xiaoying Shang, Ming Tang, **Prasenjit Dey**, Deepavali Chakravarti, Denise Spring, Patricia Troncoso, John Zhang, Y. Alan Wang, Ronald DePinho. Synthetic essentiality of chromatin remodeling factor CHD1 in PTEN deficient cancer. *Nature*, In Press.

   DOD grant (W81XWH-14-1-0429) has been acknowledged in the publication.
2. **Prasenjit Dey**, Joelle Baddour , Florian Müller , Chia Chin Wu , Huamin Wang , Wen-Ting Liao , Zangdao Lan, Nikunj Satani, Andrea Viale, Haoqiang Ying, Di Zhao, Abhinav Achreja, Lifeng Yang Qing Chang Giannicola Genovese, Alina Chen, Tony Gutschner, Ya'an Kang, Jason Fleming, Jiyoon Lee, Giulio Draetta Anirban Maitra, Y. Alan Wang, Deepak Nagrath, Ronald DePinho. Genomic deletion of malic enzyme 2 confers collateral lethality in pancreatic cancer. *Nature*, In Press.

   DOD grant (W81XWH-14-1-0429) has been acknowledged in the publication.
3. Giannicola Genovese, Alessandro Carugo, James Tepper, Frederick Scott Robinson, Liren Li, Maria Svelto, Luigi Nezi, Denise Corti, Rosalba Minelli, Piergiorgio Pettazzoni, Tony Gutschner, Chia-Chin Wu, Sahil Seth, Kadir Caner Akdemir, Elisabetta Leo, Samirkumar Amin, Marco Dal Molin, Haoqiang Ying, Lawrence Kwong, Simona Colla, Koichi Takahashi, Papia Ghosh, Virginia Giuliani, Florian Muller, **Prasenjit Dey**, Shan Jiang, Jill Garvey, Chang-Gong Liu, Jianhua Zhang, Tim Heffernan, Carlo Toniatti, Jason Fleming, Michael Goggins, Laura Wood, Alessandro Sgambato, Abbas Agaimy, Anirban Maitra, Charles W. Roberts, Huamin Wang, Andrea Viale, Ronald A. DePinho, Giulio Draetta and Lynda Chin, Therapeutic vulnerabilities of mesenchymal subpopulations of pancreatic cancer cells undergoing anabolic reprogramming. *Nature*, In Press.

   DOD grant (W81XWH-14-1-0429) has been acknowledged in the publication.
4. Sharmistha Sarkar, Christopher Bristow, **Prasenjit Dey**, Kunal Rai, Ruth Perets, Alejandra Cardenas-Ramirez Shruti Malasi, Emmet Huang-Hobbs, Monika Haemmerle, Sherry Wu, Michael McGuire, Alexei Propopotov, Shan Jiang , Jill Garvey, Joyce Liu , Michelle Hirsch, Qing Chang, Alexander Lazar, Anil Sood, Dr. Ronny Drapkin, Ronald Depinho, Giulio Draetta.

PRKCI promotes immune suppression in ovarian tumors through YAP1. *Nature Communication*, In Revision.

DOD grant (W81XWH-14-1-0429) has been acknowledged in the publication.

5. Haoqiang Ying, **Prasenjit Dey**, Wantong Yao, Alec C Kimmelman, Giulio F Draetta, Anirban Maitra, Ronald A DePinho. Genetics and biology of pancreatic ductal adenocarcinoma. *Genes & development*, 2016 Feb 15;30(4):355-85. doi: 10.1101/gad.275776.115.

   DOD grant (W81XWH-14-1-0429) has been acknowledged in the publication.
6. Cheryl L. Storer Samaniego, Ji Ho Su, Arundhati Chattopadhyay, Karen Olivares, Naihsuan Guy, Jeffrey C. Sivils, **Prasenjit Dey**, Fumiaki Yumoto, Robert J. Fletterick, Anders M. Strom, Jan-Åke Gustafsson, Paul Webb, and Marc B. Cox. The 52-kDa FK506-Binding Protein (FKBP52) Acts in Synergy with β-Catenin to Potentiate Androgen Receptor Signaling. *PLOS ONE* 10 (7), e0134015**.**

- **Website(s) or other Internet site(s)**

"Nothing to Report."

- **Technologies or techniques**

"Nothing to Report."

- **Inventions, patent applications, and/or licenses**

"Nothing to Report."

- **Other Products**

"Nothing to Report."

- *data or databases;*

The expression array data used in this article were in GEO with accession numbers GSE25140 (11) and GSE71319

-
- *biospecimen collections;*

- *audio or video products;*
- *software;*
- *models;*
- *educational aids or curricula;*
- *instruments or equipment;*
- *research material (e.g., Germplasm; cell lines, DNA probes, animal models);*
- *clinical interventions;*
- *new business creation; and*
- *other.*

7. PARTICIPANTS & OTHER COLLABORATING ORGANIZATIONS

- **What individuals have worked on the project?**

"Nothing to Report."

- **Has there been a change in the active other support of the PD/PI(s) or senior/key personnel since the last reporting period?**

"Nothing to Report."

- **What other organizations were involved as partners?**

"Nothing to Report."

8. SPECIAL REPORTING REQUIREMENTS

- **COLLABORATIVE AWARDS:**

"Nothing to Report."

- **QUAD CHARTS:**

"Nothing to Report."

9. APPENDICES:

Attached is the Cancer Discovery manuscript.

References

1. Heinlein, C.A. and C. Chang, *Androgen receptor in prostate cancer.* Endocr Rev, 2004. **25**(2): p. 276-308.
2. Karantanos, T., P.G. Corn, and T.C. Thompson, *Prostate cancer progression after androgen deprivation therapy: mechanisms of castrate resistance and novel therapeutic approaches.* Oncogene, 2013. **32**(49): p. 5501-11.
3. Sluka, P. and I.D. Davis, *Cell mates: paracrine and stromal targets for prostate cancer therapy.* Nat Rev Urol, 2013. **10**(8): p. 441-51.
4. Lindau, D., et al., *The immunosuppressive tumour network: myeloid-derived suppressor cells, regulatory T cells and natural killer T cells.* Immunology, 2013. **138**(2): p. 105-15.
5. Solito, S., et al., *Highlights on molecular mechanisms of MDSC-mediated immune suppression: paving the way for new working hypotheses.* Immunol Invest, 2012. **41**(6-7): p. 722-37.
6. Gabrilovich, D.I. and S. Nagaraj, *Myeloid-derived suppressor cells as regulators of the immune system.* Nat Rev Immunol, 2009. **9**(3): p. 162-74.
7. Joyce, J.A. and J.W. Pollard, *Microenvironmental regulation of metastasis.* Nat Rev Cancer, 2009. **9**(4): p. 239-52.
8. Sawant, A. and S. Ponnazhagan, *Myeloid-derived suppressor cells as osteoclast progenitors: a novel target for controlling osteolytic bone metastasis.* Cancer Res, 2013. **73**(15): p. 4606-10.
9. Ammirante, M., et al., *B-cell-derived lymphotoxin promotes castration-resistant prostate cancer.* Nature, 2010. **464**(7286): p. 302-5.
10. Nelson, B.H., *CD20+ B cells: the other tumor-infiltrating lymphocytes.* J Immunol, 2010. **185**(9): p. 4977-82.
11. Shojaei, F., et al., *Tumor refractoriness to anti-VEGF treatment is mediated by CD11b+Gr1+ myeloid cells.* Nat Biotechnol, 2007. **25**(8): p. 911-20.
12. Finke, J., et al., *MDSC as a mechanism of tumor escape from sunitinib mediated anti-angiogenic therapy.* Int Immunopharmacol, 2011. **11**(7): p. 856-61.
13. Lunardi, A., et al., *A co-clinical approach identifies mechanisms and potential therapies for androgen deprivation resistance in prostate cancer.* Nat Genet, 2013. **45**(7): p. 747-55.
14. Wang, G., et al., *Zbtb7a suppresses prostate cancer through repression of a Sox9-dependent pathway for cellular senescence bypass and tumor invasion.* Nat Genet, 2013. **45**(7): p. 739-46.
15. Bendall, S.C., et al., *Single-cell mass cytometry of differential immune and drug responses across a human hematopoietic continuum.* Science, 2011. **332**(6030): p. 687-696.
16. Talmadge, J.E. and D.I. Gabrilovich, *History of myeloid-derived suppressor cells.* Nat Rev Cancer, 2013. **13**(10): p. 739-52.
17. Idorn, M., et al., *Correlation between frequencies of blood monocytic myeloid-derived suppressor cells, regulatory T cells and negative prognostic markers in patients with castration-resistant metastatic prostate cancer.* Cancer Immunol Immunother, 2014. **63**(11): p. 1177-87.
18. Kusmartsev, S., et al., *Antigen-specific inhibition of CD8+ T cell response by immature myeloid cells in cancer is mediated by reactive oxygen species.* J Immunol, 2004. **172**(2): p. 989-99.
19. Schmielau, J. and O.J. Finn, *Activated granulocytes and granulocyte-derived hydrogen peroxide are the underlying mechanism of suppression of t-cell function in advanced cancer patients.* Cancer Res, 2001. **61**(12): p. 4756-60.
20. Ding, Z., et al., *SMAD4-dependent barrier constrains prostate cancer growth and metastatic progression.* Nature, 2011. **470**(7333): p. 269-73.
21. Yang, L., et al., *Abrogation of TGF beta signaling in mammary carcinomas recruits Gr-1+CD11b+ myeloid cells that promote metastasis.* Cancer Cell, 2008. **13**(1): p. 23-35.
22. Johnson, R. and G. Halder, *The two faces of Hippo: targeting the Hippo pathway for regenerative medicine and cancer treatment.* Nat Rev Drug Discov, 2014. **13**(1): p. 63-79.
23. Zhao, B., et al., *Cell detachment activates the Hippo pathway via cytoskeleton reorganization to induce anoikis.* Genes Dev, 2012. **26**(1): p. 54-68.
24. Nguyen, L.T., et al., *ERG Activates the YAP1 Transcriptional Program and Induces the Development of Age-Related Prostate Tumors.* Cancer Cell, 2015. **27**(6): p. 797-808.

25. Kwon, A.T., et al., *oPOSSUM-3: advanced analysis of regulatory motif over-representation across genes or ChIP-Seq datasets.* G3 (Bethesda), 2012. **2**(9): p. 987-1002.

ABSTRACT The signaling mechanisms between prostate cancer cells and infiltrating immune cells may illuminate novel therapeutic approaches. Here, utilizing a prostate adenocarcinoma model driven by loss of *Pten* and *Smad4*, we identify polymorphonuclear myeloid-derived suppressor cells (MDSC) as the major infiltrating immune cell type, and depletion of MDSCs blocks progression. Employing a novel dual reporter prostate cancer model, epithelial and stromal transcriptomic profiling identified CXCL5 as a cancer-secreted chemokine to attract CXCR2-expressing MDSCs, and, correspondingly, pharmacologic inhibition of CXCR2 impeded tumor progression. Integrated analyses identified hyperactivated Hippo–YAP signaling in driving CXCL5 upregulation in cancer cells through the YAP–TEAD complex and promoting MDSC recruitment. Clinicopathologic studies reveal upregulation and activation of YAP1 in a subset of human prostate tumors, and the YAP1 signature is enriched in primary prostate tumor samples with stronger expression of MDSC-relevant genes. Together, YAP-driven MDSC recruitment via heterotypic CXCL5–CXCR2 signaling reveals an effective therapeutic strategy for advanced prostate cancer.

SIGNIFICANCE: We demonstrate a critical role of MDSCs in prostate tumor progression and discover a cancer cell nonautonomous function of the Hippo–YAP pathway in regulation of CXCL5, a ligand for CXCR2-expressing MDSCs. Pharmacologic elimination of MDSCs or blocking the heterotypic CXCL5–CXCR2 signaling circuit elicits robust antitumor responses and prolongs survival. *Cancer Discov; 6(1); 1–16. ©2015 AACR.*

INTRODUCTION

The tumor microenvironment (TME) is comprised of a complex mixture of tumor-associated fibroblasts, infiltrating immune cells, endothelial cells, extracellular matrix proteins, and signaling molecules, such as cytokines (1–3). Homotypic and heterotypic interactions between these cellular constituents play essential roles in cancer development and response to therapeutics (3, 4). Among the infiltrating immune cells, myeloid-derived suppressor cells (MDSC) represent a phenotypically heterogeneous population of immature myeloid cells that play a tumor-promoting role by maintaining a state of immunologic anergy and tolerance (5). In particular, activated MDSCs provide a source of secreted chemokines, cytokines, and enzymes, which suppress local T-cell activation and viability (5). In addition, MDSCs can suppress T-cell activity through deprivation of nutrients, such as L-arginine and L-cysteine, and interference with T-cell receptor functions via reactive oxygen species (ROS) and reactive nitrogen species.

Prostate cancer is the most common noncutaneous malignancy in men in the United States. Similar to many other solid tumor types, prostate cancer is characterized by a rich tumor–stroma interaction network that forms the TME (1–3). In prostate cancer, various signaling pathways have been implicated in the cross-talk between tumor and stroma, such as androgen receptor signaling, FGF, SRC, TGFβ, IGF, integrin, and Hedgehog pathways (1). Interestingly, MDSC abundance in the blood correlates with circulating PSA levels in patients with prostate cancer (6–8). MDSCs have been identified recently as a TME constituent in an indolent prostate cancer mouse model with conditional *Pten* deletion (9) and demonstrated to antagonize senescence during early tumorigenesis (10). However, the molecular mechanisms underlying the recruitment of MDSCs are not well understood, and the extent to which MDSCs facilitate prostate cancer progression has not been determined.

Previously, we have shown that deletion of *Pten* in the mouse prostate causes upregulation of SMAD4, which constrains cell proliferation and invasion, and, accordingly, dual deletion of *Pten* and *Smad4* results in rapid prostate cancer progression, including metastasis (11). Comparative transcriptomic and cell profile analyses of PTEN- versus PTEN/SMAD4–deficient prostate cancer revealed a prominent immune signature and resident MDSCs as a major TME population in PTEN/SMAD4–deficient tumors. Biologic, molecular, and pharmacologic analyses established that a YAP1-mediated CXCL5–CXCR2 signaling axis recruits MDSCs into the TME and that

---

[1]Department of Cancer Biology, The University of Texas MD Anderson Cancer Center, Houston, Texas. [2]Department of Genomic Medicine, The University of Texas MD Anderson Cancer Center, Houston, Texas. [3]Institute for Applied Cancer Science, The University of Texas MD Anderson Cancer Center, Houston, Texas. [4]Sun Yat-Sen University Cancer Center, Guangzhou, People's Republic of China. [5]Department of Genitourinary Medical Oncology, The University of Texas MD Anderson Cancer Center, Houston, Texas. [6]Department of Biological Science, College of Natural Sciences, Wonkwang University, Cheonbuk, Iksan, South Korea. [7]Sanofi Oncology, Cambridge, Massachusetts. [8]Department of Pathology, The University of Texas MD Anderson Cancer Center, Houston, Texas. [9]Department of Veterinary Medicine and Surgery, The University of Texas MD Anderson Cancer Center, Houston, Texas.

Note: Supplementary data for this article are available at Cancer Discovery Online (http://cancerdiscovery.aacrjournals.org/).

G. Wang and X. Lu contributed equally to this article.

Corresponding Authors: Y. Alan Wang, The University of Texas MD Anderson Cancer Center, 1515 Holcombe Boulevard, Houston, TX 77030. Phone: 713-792-7928; Fax: 713-794-4005; E-mail: yalanwang@mdanderson.org; and Ronald A. DePinho, Phone: 713-792-6000, rdepinho@mdanderson.org

doi: 10.1158/2159-8290.CD-15-0224

MDSCs play critical roles in facilitating tumor progression. Our comprehensive analyses using a prostate cancer model coupled with clinical validation using patient samples support the view that targeting either MDSC recruitment or infiltrated MDSCs may represent a valid therapeutic opportunity in treating advanced prostate cancer.

RESULTS

Prominent Infiltration of Immune Cells in the *Pten*$^{pc-/-}$*Smad4*$^{pc-/-}$ Tumor Model

We previously reported that conditional deletion of *Smad4* bypassed the senescence barrier instigated by *Pten* loss in the prostate epithelia, resulting in a highly proliferative and invasive prostate adenocarcinoma characterized by an exuberant stromal reaction and frequent metastasis to distant organs (11). Correspondingly, ingenuity pathway analysis (IPA) revealed prominent representation of cell movement, cell proliferation, and antigen presentation as the top three categories represented in the *Pten*$^{pc-/-}$*Smad4*$^{pc-/-}$ tumors (11). Further analysis revealed a prominent immune signature, including Granulocytes Adhesion and Diapedesis, Leukocytes Extravasation Signaling, and Agrandulocytes Adhesion and Diapedesis as three of the top four most activated pathways in *Pten*$^{pc-/-}$*Smad4*$^{pc-/-}$ tumors compared with those present in *Pten*$^{pc-/-}$ tumors (Fig. 1A; P value < 2.03E−7). Correspondingly, IHC staining highlighted conspicuous infiltration of CD45$^+$ leukocytes in *Pten*$^{pc-/-}$*Smad4*$^{pc-/-}$ tumors (Fig. 1B). To comprehensively audit the spectrum of infiltrating immune cells in tumors, we performed mass cytometry (CyTOF) immunophenotyping (12) to catalog tumor cell–type constituents from well-established tumors in 16-week-old *Pten*$^{pc-/-}$ and *Pten*$^{pc-/-}$*Smad4*$^{pc-/-}$ mice. Employing a 9-marker antibody panel (Supplementary Table S1), CyTOF confirmed a significant increase in CD45$^+$-infiltrating leukocytes in *Pten*$^{pc-/-}$*Smad4*$^{pc-/-}$ as compared with *Pten*$^{pc-/-}$ tumors (Fig. 1C). Within the CD45$^+$-infiltrating cells, CD11b$^+$ myeloid cells represented a significantly increased immune population in *Pten*$^{pc-/-}$*Smad4*$^{pc-/-}$ as compared with *Pten*$^{pc-/-}$ tumors (Fig. 1D).

CD11b$^+$Gr1$^+$ Cells Are Significantly Increased in *Pten*$^{pc-/-}$*Smad4*$^{pc-/-}$ Tumor Model

To obtain a dynamic view of peripheral and infiltrating immune cells as a function of tumor progression in the *Pten*$^{pc-/-}$*Smad4*$^{pc-/-}$ model, which initiates tumor development at 6 to 8 weeks and progresses to early invasive carcinoma by 14 weeks of age, serial CyTOF analyses using an expanded antibody panel of 17 surface markers (Supplementary Table S1) were performed on single cells from primary tumors, peripheral blood, spleen, and draining lymph nodes at 5, 8, and 14 weeks of age. The detailed immunophenotyping profiles enabled construction of the spanning-tree progression analysis of density-normalized events (SPADE)–derived tree (12). SPADE is a computational approach to facilitate the identification and analysis of heterogeneous cell types. SPADE of the *Pten*$^{pc-/-}$*Smad4*$^{pc-/-}$ model displays the complexity of the TME, which is composed of epithelial tumor cells (EpCAM$^+$CD45$^-$), nonimmune TME cells (EpCAM$^-$CD45$^-$), and infiltrating immune cells (EpCAM$^-$CD45$^+$) that can be further grouped into various immune cell subpopulations (Fig. 2A and Supplementary Fig. S1A). Among the infiltrating immune cells, there was a striking age-dependent increase of CD11b$^+$Gr1$^+$ cells in tumors (Fig. 2B) and peripheral blood from *Pten*$^{pc-/-}$*Smad4*$^{pc-/-}$ mice (Fig. 2C); this trend was much less pronounced in the spleen or draining lymph nodes (Supplementary Fig. S1B; for gating strategy, see Supplementary Fig. S1C).

CD11b$^+$Gr1$^+$ Cells from *Pten*$^{pc-/-}$*Smad4*$^{pc-/-}$ Tumors Are Potently Immunosuppressive

To evaluate the potential immunosuppressive activity of intratumoral CD11b$^+$Gr1$^+$ cells from *Pten*$^{pc-/-}$*Smad4*$^{pc-/-}$ tumors, we examined T-cell proliferation using a standard cell coculture system. These CD11b$^+$Gr1$^+$ cells strongly suppressed CD3 and CD28 antibody-induced T-cell proliferation and activation (Fig. 3A and B; see Supplementary Fig. S2 for cell isolation strategy), establishing that CD11b$^+$Gr1$^+$ cells are indeed functional MDSCs.

MDSCs can be further classified as a Ly6G$^+$Ly6C^{lo} subset with polymorphonuclear phenotype (PMN-MDSC) and a Ly6G$^-$Ly6C^{hi} subset with monocytic phenotype (M-MDSC; ref. 13). PMN-MDSCs represented the major MDSC population in *Pten*$^{pc-/-}$*Smad4*$^{pc-/-}$ tumors (Fig. 3C and D), consistent with previously observed preferential expansion of PMN-MDSCs in tumor-bearing mice of various syngeneic models (5, 9, 13). The abundance of PMN-MDSCs was further confirmed by IHC for Ly6G, as shown by quantification of both intraepithelial and stromal Ly6G$^+$ cells in tumors from *Pten*$^{pc-/-}$*Smad4*$^{pc-/-}$ mice and *Pten*$^{pc-/-}$ mice (Fig. 3E and F). It has been shown previously that ROS production by PMN-MDSCs is one of the mechanisms driving immune suppression (5, 14–16). Correspondingly, IPA revealed that pathways involved in ROS and nitric oxide (NO) production are among the top pathways activated in *Pten*$^{pc-/-}$*Smad4*$^{pc-/-}$ tumors (Fig. 1A, arrow). Consistent with the increased infiltration of PMN-MDSCs in the *Pten*$^{pc-/-}$*Smad4*$^{pc-/-}$ tumors, the expression of several subunits of NADPH oxidase (*Nox2*, *p40*^{phox}, and *p47*^{phox}), which are responsible for ROS production in PMN-MDSCs (5), was significantly upregulated in *Pten*$^{pc-/-}$*Smad4*$^{pc-/-}$ tumors relative to *Pten*$^{pc-/-}$ tumors (Fig. 3G). Moreover, *Arg1*, but not *Nos2*, was highly upregulated in the *Pten*$^{pc-/-}$*Smad4*$^{pc-/-}$ tumors (Fig. 3G). Together, MDSCs in autochthonous *Pten*$^{pc-/-}$*Smad4*$^{pc-/-}$ tumors display strong T-cell–suppressive activity and are predominantly the PMN-MDSC subtype.

Immunodepletion of MDSCs Impedes Tumor Progression in *Pten*$^{pc-/-}$*Smad4*$^{pc-/-}$ Mice

Enrichment of MDSCs in advanced *Pten*$^{pc-/-}$*Smad4*$^{pc-/-}$ tumors prompted us to explore the possible role of MDSCs in tumor progression. Using a well-characterized anti-Gr1 neutralizing monoclonal antibody (clone RB6-8C5; ref. 17), MDSCs were depleted in *Pten*$^{pc-/-}$*Smad4*$^{pc-/-}$ mice at 14 weeks of age, a point coincident with progression to the early invasive carcinoma stage (see Supplementary Fig. S3A for treatment scheme). The potent MDSC depletion activity of anti-Gr1 monoclonal antibody was evidenced by significantly decreased PMN-MDSCs and M-MDSCs in peripheral blood as early as day 2 after treatment (Supplementary Fig. S3B). In

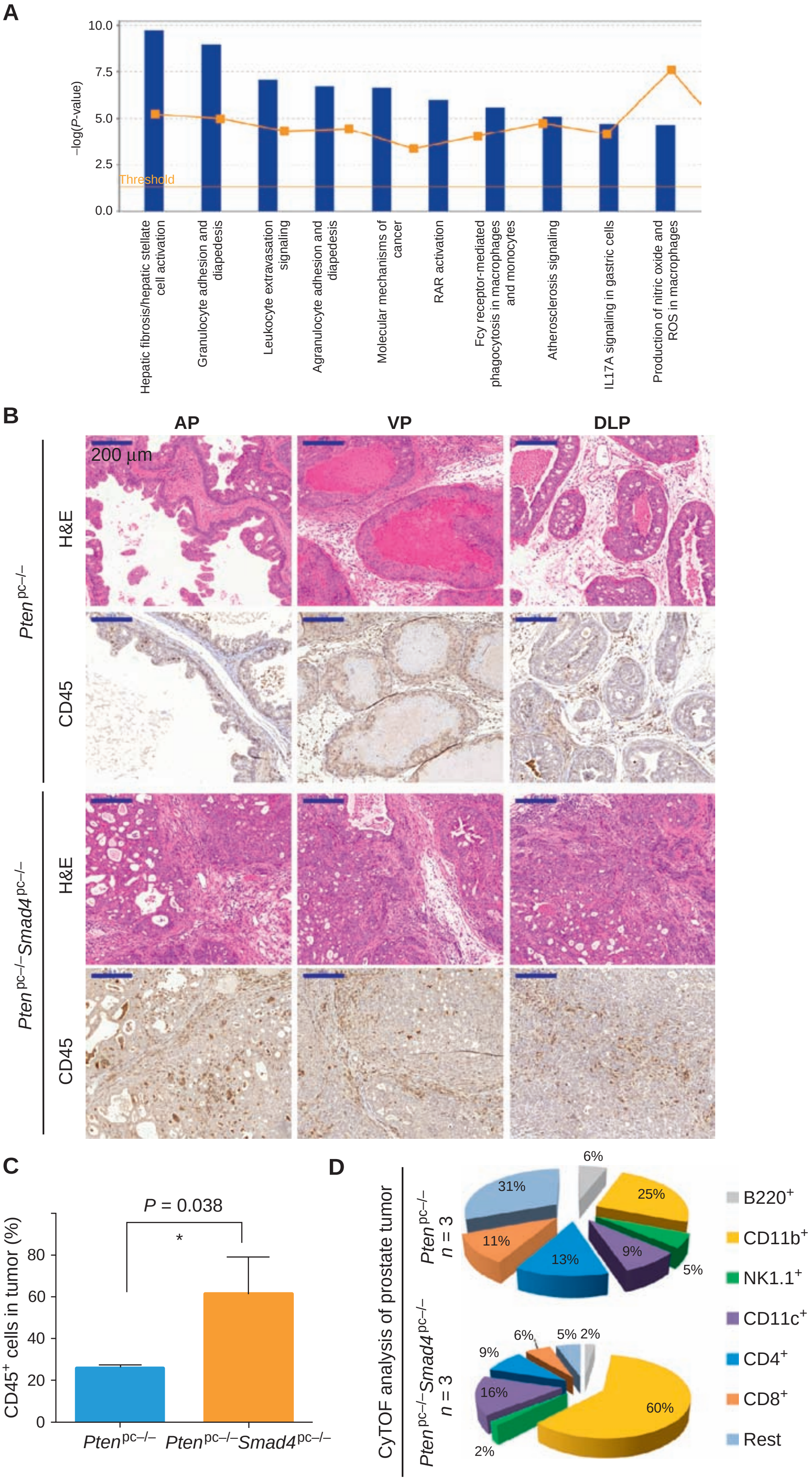

Figure 1. Prominent infiltration of immune cells in the *Pten*$^{pc-/-}$*Smad4*$^{pc-/-}$ tumors as compared with *Pten*$^{pc-/-}$ tumors. **A,** the top 10 activated pathways in *Pten*$^{pc-/-}$*Smad4*$^{pc-/-}$ tumors ($n = 5$) as compared with *Pten*$^{pc-/-}$ tumors ($n = 5$) identified by IPA. RAR, retinoic acid receptor. **B,** a significant increase in the infiltration of immune cells as shown by IHC for CD45 in *Pten*$^{pc-/-}$*Smad4*$^{pc-/-}$ tumors as compared with *Pten*$^{pc-/-}$ tumors from 16-week-old mice ($n = 3$). AP, anterior prostate; VP, ventral prostate; DLP, dorsolateral prostate; H&E, hematoxylin and eosin staining. Scale bars, 200 µm. **C,** quantification of tumor-infiltrating CD45$^+$ cells (AP, VP, and DLP combined) in *Pten*$^{pc-/-}$ tumors and *Pten*$^{pc-/-}$*Smad4*$^{pc-/-}$ from 16-week-old mice ($n = 3$), assessed by CyTOF. **D,** percentages of various immune cell populations within the CD45$^+$-infiltrating immune cells in prostate tumors from 16-week-old *Pten*$^{pc-/-}$ and *Pten*$^{pc-/-}$*Smad4*$^{pc-/-}$ mice, assessed with CyTOF (9-marker) and analyzed with FlowJo. CD11b$^+$ myeloid cells are significantly greater in *Pten*$^{pc-/-}$*Smad4*$^{pc-/-}$ tumors as compared with *Pten*$^{pc-/-}$ tumors ($n = 3$; $P < 0.05$).

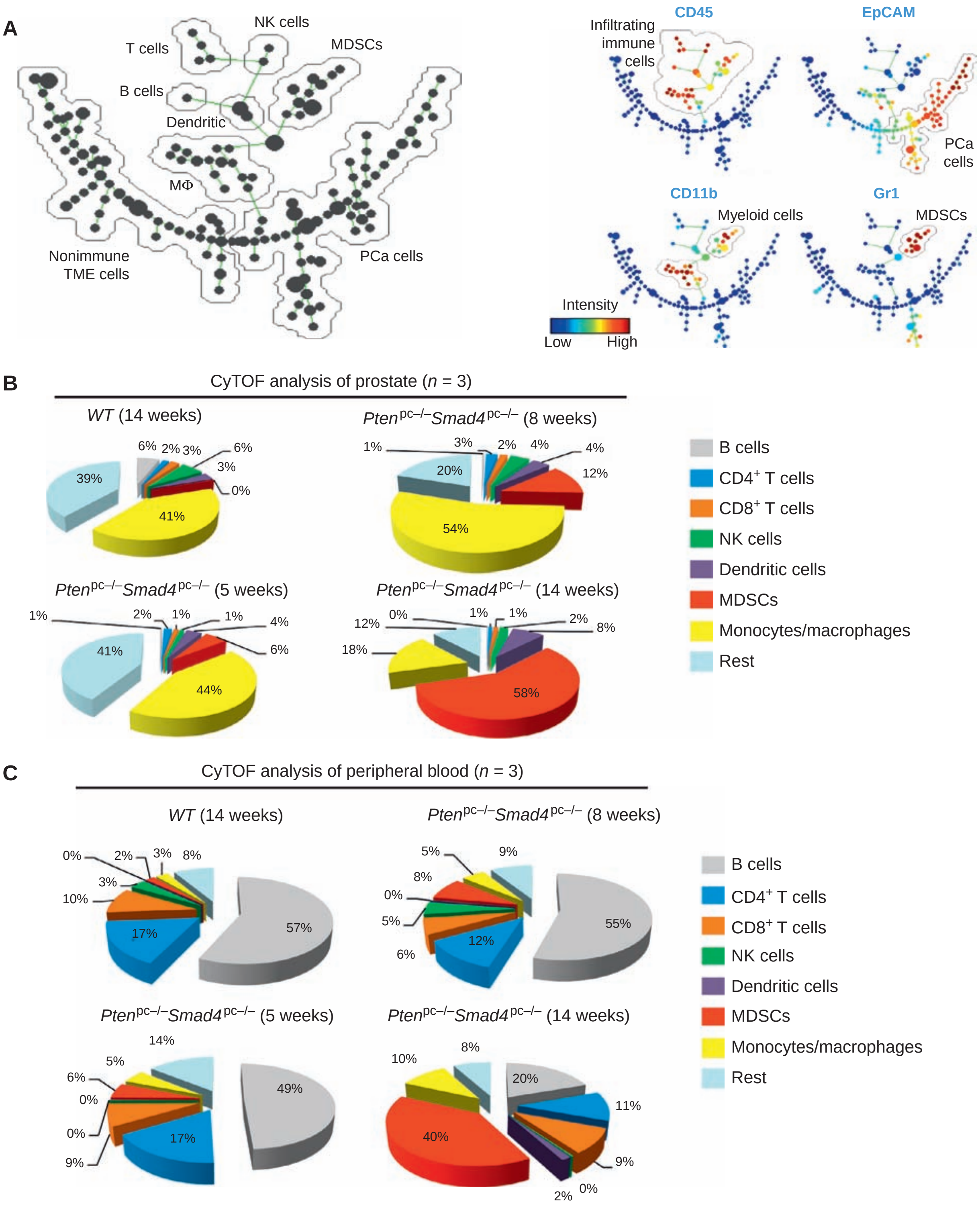

Figure 2. CD11b$^+$Gr1$^+$ cells are significantly increased in $Pten^{pc-/-}Smad4^{pc-/-}$ tumors as compared with $Pten^{pc-/-}$ tumors. **A,** SPADE tree derived from CyTOF (17-marker) analysis of whole-tumor cell population from $Pten^{pc-/-}Smad4^{pc-/-}$ mice at 5 weeks, 8 weeks, and 14 weeks of age ($n = 3$). Live single cells were used to construct the tree. Cell populations were identified as prostate cancer (PCa) cells (EpCAM$^+$CD45$^-$), nonimmune TME cells (EpCAM$^-$CD45$^-$), T cells (CD45$^+$CD3$^+$TCRβ$^+$), B cells (CD45$^+$B220$^+$CD19$^+$), natural killer (NK) cells (CD45$^+$NK1.1$^+$), dendritic cells (CD45$^+$CD11c$^+$), putative MDSCs (CD45$^+$CD11b$^+$Gr1$^+$), and macrophages (CD45$^+$CD11b$^+$Gr1$^-$). On the right plots, the tree is colored by the median intensity of individual markers shown on the top to highlight infiltrating immune cells (EpCAM$^-$CD45$^+$), epithelial prostate cancer cells (EpCAM$^+$CD45$^-$), total myeloid cells (CD45$^+$CD11b$^+$), and putative MDSCs (CD45$^+$CD11b$^+$Gr1$^+$). **B** and **C,** CyTOF analysis of tumors (**B**) or peripheral blood (**C**) from 5-, 8-, and 14-week-old $Pten^{pc-/-}Smad4^{pc-/-}$ mice revealed an age-dependent increase in the MDSC infiltration. Prostate from wild-type (WT) mice at 16 weeks old was used as control ($n = 3$ for each genotype). See also Supplementary Fig. S1.

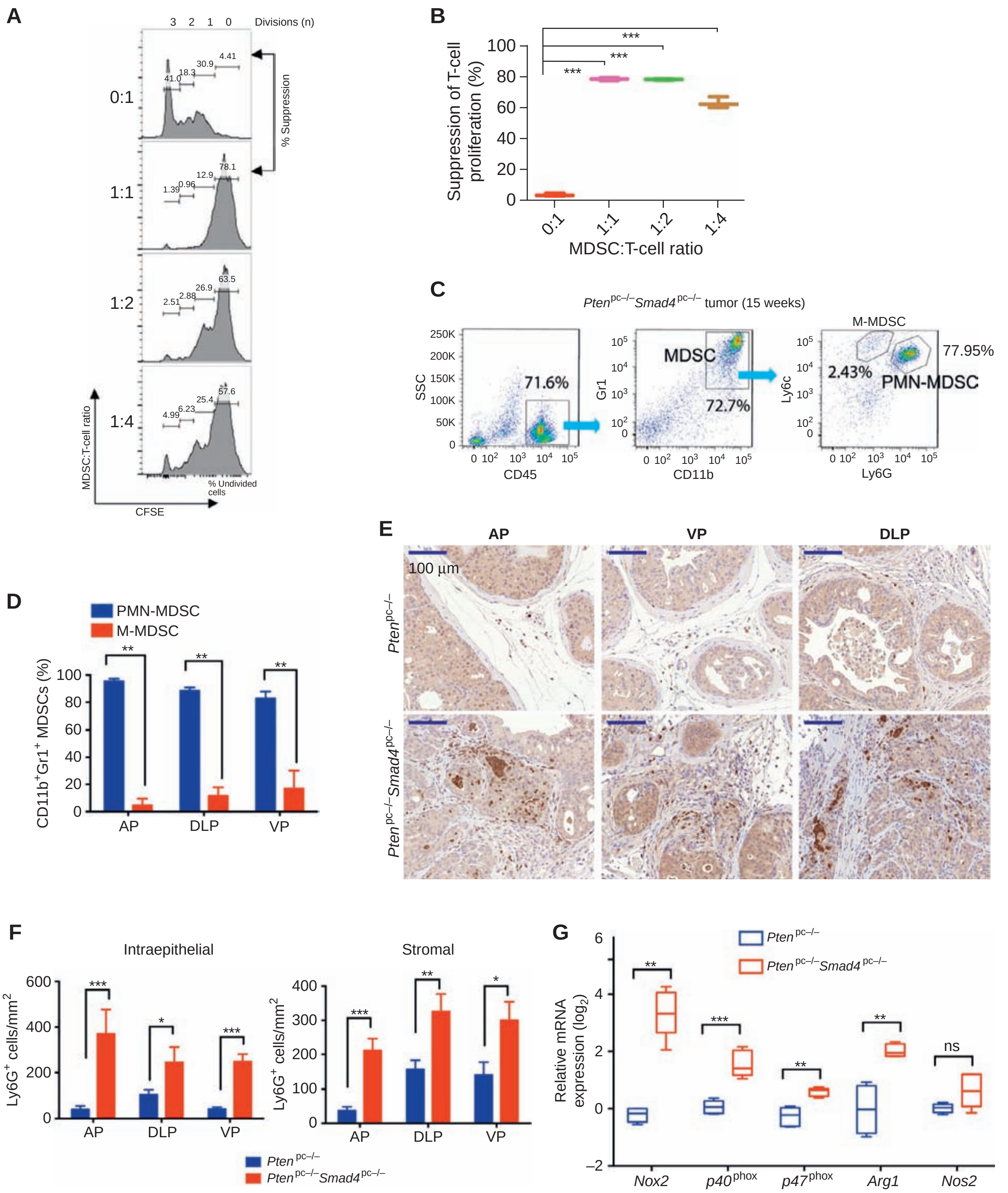

Figure 3. MDSCs from *Pten*$^{pc-/-}$*Smad4*$^{pc-/-}$ tumors display potent immunosuppressive activities and are dominated by PMN-MDSCs. **A,** CD11b^{+}Gr1^{+} cells from *Pten*$^{pc-/-}$*Smad4*$^{pc-/-}$ tumors display potent immune-suppressive activity toward T-cell activation as demonstrated by CFSE dilution assay in triplicate. **B,** summarized result from **A**. **C** and **D,** flow cytometry analysis shows PMN-MDSCs as the major population in the infiltrated MDSCs in established *Pten*$^{pc-/-}$*Smad4*$^{pc-/-}$ tumors at AP, DLP, and VP ($n = 5$). SSC, side scatter. **E** and **F,** a significant increase in Ly6G^{+} cells in *Pten*$^{pc-/-}$*Smad4*$^{pc-/-}$ tumors as compared with the *Pten*$^{pc-/-}$ tumors as shown by IHC for Ly6G and quantified by location of positively stained cells in the intraepithelial or stromal compartment of the tumor at AP, DLP, and VP ($n = 3$). **G,** quantification of the mRNA expression of subunits of NADPH oxidase (*Nox2*, *p40*^{phox}, and *p47*^{phox}), *Arg1*, and *Nos2* in the *Pten*$^{pc-/-}$*Smad4*$^{pc-/-}$ tumors and the *Pten*$^{pc-/-}$ tumors ($n = 5$). In **B, D, F,** and **G,** *, $P < 0.05$; **, $P < 0.01$; ***, $P < 0.001$; ns, nonsignificant. Also see Supplementary Fig. S2.

addition, a systemic reduction of MDSCs in spleen, bone marrow, and prostate tumors was documented following a 30-day treatment regimen of anti-Gr1 monoclonal antibody (Fig. 4A and Supplementary Fig. S3C). This MDSC depletion was accompanied by an increase of CD8$^+$ T cells (so-called killer T cells; Fig. 4A), consistent with elimination of the T-cell suppression activity of MDSCs. Importantly, in line with the CD8$^+$ T-cell expansion, we observed that the Gr1-treated prostate displayed remarkable weight reduction in ventral and dorsolateral prostates (VP and DLP; Fig. 4B). The lack of difference in the weight of the anterior prostate (AP) is likely due to the fact that the AP tends to develop cysts with fluid accumulated inside the gland (18, 19), which also prevents the accurate measure of the prostate weight (Supplementary Fig. S3D). Histopathologic analysis revealed adenocarcinoma was the predominant pathology in mice treated with the control IgG, whereas mouse prostatic intraepithelial neoplasia (mPIN) was the predominant morphologic presentation in prostates from mice treated with anti-Gr1 monoclonal antibody (Fig. 4C and Supplementary Table S2). In addition, by immunohistochemical staining for CD45, Ki67, vimentin, smooth muscle actin (SMA), and Trichrome staining, we observed that tumor remnants in mice treated with anti-Gr1 monoclonal antibody displayed markedly reduced levels of cellular proliferation, stromal reaction, and inflammation as compared with those tumors treated with control IgG antibody (Supplementary Fig. S4A).

In another therapeutic trial, we also utilized the recently developed MDSC-specific peptide–Fc fusion protein (i.e., peptibodies) that has been shown to effectively eliminate MDSCs *in vivo* through targeting the S100A9 surface protein (20). Employing a hydrodynamic injection approach for nucleic acid delivery (21), intravenous injection of either Pep-H6 peptibody expression vector or irrelevant control peptibody vector was initiated at 14 weeks every 4 days in *Pten*$^{pc-/-}$*Smad4*$^{pc-/-}$ mice. Strikingly, a single injection of the Pep-H6 peptibody significantly reduced the MDSCs in the peripheral blood, whereas such effect was not observed using the irrelevant control peptibody (Supplementary Fig. S4B). Pep-H6 peptibody treatment for 1 month led to a dramatic decrease in cancer cell content in the prostate tumors (Fig. 4D) and provided significant survival benefit for tumor-bearing mice (Fig. 4E). Together, our data strongly support the view that MDSC depletion blocks prostate tumor progression in the *Pten*$^{pc-/-}$*Smad4*$^{pc-/-}$ model.

CXCL5–CXCR2 Signaling Promotes MDSC Recruitment and CXCR2 Inhibition Delays Tumor Progression in *Pten*$^{pc-/-}$*Smad4*$^{pc-/-}$ Mice

To elucidate the cellular origins and signaling molecules governing MDSC recruitment to prostate tumors, we incorporated the *mTmG* dual fluorescence reporter allele into the *Pten*$^{pc-/-}$*Smad4*$^{pc-/-}$ model where signaling events between tumor cells and stroma can be precisely delineated. The *mTmG* allele (22) allows Cre-dependent GFP expression in prostate epithelial cells and ubiquitous tdTomato expression in all other non–Cre-expressing cells (Fig. 5A). Transcriptomic and IPA analyses of FACS-sorted GFP$^+$ tumor cells and Tomato$^+$ stromal cells showed distinct expression patterns by hierarchical clustering (Fig. 5A) with tumor cells enriched for pathways involved in cell adhesion molecules and tight junctions (consistent with their epithelial nature) and stromal cells displaying activation of more diverse pathways involved in chronic inflammation, such as cytokine/cytokine receptor interaction, chemokine, JAK–STAT, T-cell repector, and B-cell receptor signaling ($P < 0.01$, data not shown). This result is consistent with the immunopathologic and histopathologic analyses showing a massive infiltration of immune cells in the *Pten*$^{pc-/-}$*Smad4*$^{pc-/-}$ tumors.

Employing this new model, we sought to identify genes that were upregulated in *Pten*$^{pc-/-}$*Smad4*$^{pc-/-}$ cancer cells relative to *Pten*$^{pc-/-}$ cancer cells that might illuminate mechanisms involved in the recruitment of MDSCs by classifying the upregulated genes into either stroma- or tumor-enriched genes. To this end, our previously generated list of 242 genes with greater than 2-fold increased expression in *Pten*$^{pc-/-}$*Smad4*$^{pc-/-}$ relative to *Pten*$^{pc-/-}$ tumors (11) was intersected with 486 genes preferentially expressed in *Pten*$^{pc-/-}$*Smad4*$^{pc-/-}$ GFP$^+$ cancer cells relative to Tomato$^+$ stroma cells (fold change ≥4; Supplementary Tables S3 and S4), yielding 28 genes that are markedly enriched in *Pten*$^{pc-/-}$*Smad4*$^{pc-/-}$ cancer cells (Supplementary Table S5). Among these 28 genes, *Cxcl5*, which encodes a key cytokine involved in MDSC recruitment (23, 24), is the most significantly upregulated cancer cell–specific cytokine in *Pten*$^{pc-/-}$*Smad4*$^{pc-/-}$ tumors as compared with *Pten*$^{pc-/-}$ tumors (Fig. 5B and Supplementary Fig. S5A). Notably, CXCR2, the cognate receptor for CXCL5, is also upregulated in *Pten*$^{pc-/-}$*Smad4*$^{pc-/-}$ tumors as compared with *Pten*$^{pc-/-}$ tumors and is significantly enriched in *Pten*$^{pc-/-}$*Smad4*$^{pc-/-}$ Tomato$^+$ stroma cells (Fig. 5B). The upregulation of CXCL5 expression in *Pten*$^{pc-/-}$*Smad4*$^{pc-/-}$ prostate tumors was further confirmed by IHC (Fig. 5C). In addition, we performed FACS analysis of CD11b$^+$Gr1$^+$ cells and CD11b$^-$Gr1$^-$ cells from bone marrow, spleen, peripheral blood, and tumors for CXCR2 expression. As shown in Supplementary Fig. S5B, CD11b$^-$Gr1$^-$ cells (largely lymphocytes) are devoid of CXCR2 expression, whereas a large fraction of CD11b$^+$Gr1$^+$ cells express CXCR2. When CXCR2 expression was further separated into CXCR2^{hi} and CXCR2$^+$, we observed an enrichment of the CXCR2^{hi} subpopulation in the CD11b$^+$Gr1$^+$ cells in prostate tumors compared with CD11b$^+$Gr1$^+$ cells from bone marrow, spleen, or blood (Supplementary Fig. S5B). This is consistent with the model of active recruitment of MDSCs by tumors through CXCR2-mediated chemoattraction.

To validate the CXCL5–CXCR2 axis in the recruitment of MDSCs to the TME of *Pten*$^{pc-/-}$*Smad4*$^{pc-/-}$ tumors, we assessed the impact of pharmacologic inhibition of CXCL5 and CXCR2 in MDSCs using a transwell migration assay (23). First, anti–CXCL5-neutralizing antibody pretreatment of conditioned medium (CM) derived from *Pten*$^{pc-/-}$*Smad4*$^{pc-/-}$ prostate cancer cell line resulted in decreased migration of MDSCs (Fig. 5D). Second, CXCR2 inhibitor SB255002 or anti-CXCR2 neutralizing antibody pretreatment also impeded migration of MDSCs (Fig. 5D). Third, *in vivo* blockade of the CXCL5–CXCR2 axis using SB255002 in 14-week-old *Pten*$^{pc-/-}$*Smad4*$^{pc-/-}$ mice over a 14-day daily dosing schedule revealed a dramatic reduction in infiltration of MDSCs in the prostate tumors (Supplementary Fig. S5C and S5D). Notably, similar to mice treated with anti-Gr1 neutralizing antibody, these SB225002-treated *Pten*$^{pc-/-}$*Smad4*$^{pc-/-}$ mice also showed significant reduction in tumor burden (VP and DLP) as compared with the vehicle-treated controls (Fig. 5E and Supplementary Fig. S5E). Strikingly,

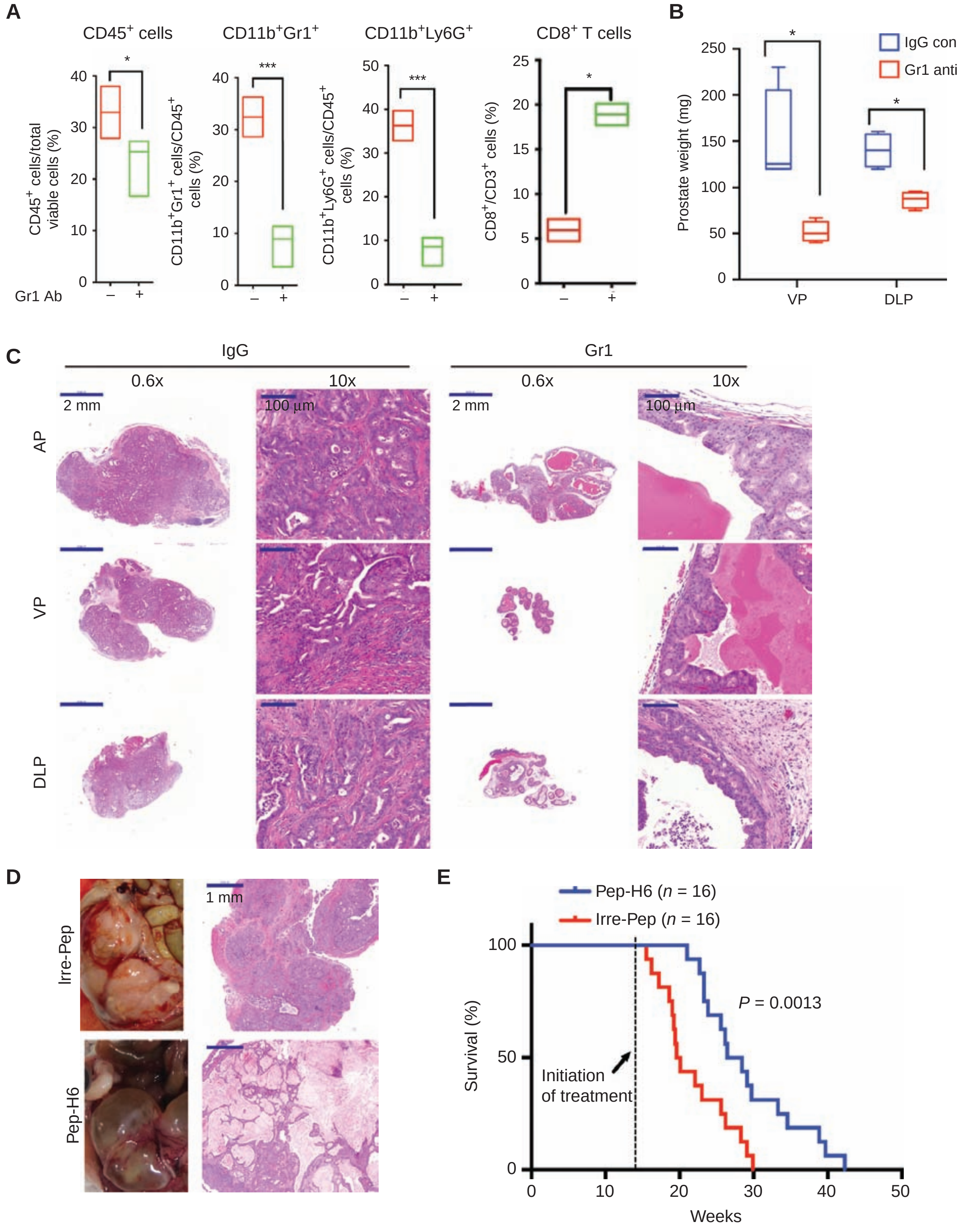

Figure 4. Targeting MDSCs with anti-Gr1 neutralizing antibody or MDSC-specific peptibody significantly delayed tumor progression in *Pten*$^{pc-/-}$*Smad4*$^{pc-/-}$ mice. **A,** administration of Gr1-neutralizing antibody *in vivo* significantly reduced CD45$^+$-infiltrating immune cells, reduced MDSCs, and increased CD8$^+$ T cells among total T cells in *Pten*$^{pc-/-}$*Smad4*$^{pc-/-}$ tumors ($n = 4$), measured by flow cytometry. **B,** Gr1 antibody treatment of 14-week-old mice significantly reduced the weight of VP and DLP in *Pten*$^{pc-/-}$*Smad4*$^{pc-/-}$ mice. **C,** Gr1 antibody remarkably altered the tumor histopathology in *Pten*$^{pc-/-}$*Smad4*$^{pc-/-}$ adenocarcinoma, analyzed by hematoxylin and eosin staining of AP, VP, and DLP. **D,** one month of Pep-H6 peptibody treatment led to significant appearance and histology changes of the *Pten*$^{pc-/-}$*Smad4*$^{pc-/-}$ adenocarcinoma. Irre-Pep, irrelevant control peptibody. **E,** Kaplan–Meier survival curve showing the significant delay of mortality caused by Pep-H6 peptibody treatment of *Pten*$^{pc-/-}$*Smad4*$^{pc-/-}$ mice. In **A** and **B,** *, $P < 0.05$ and ***, $P < 0.001$; Also see Supplementary Figs. S3 and S4.

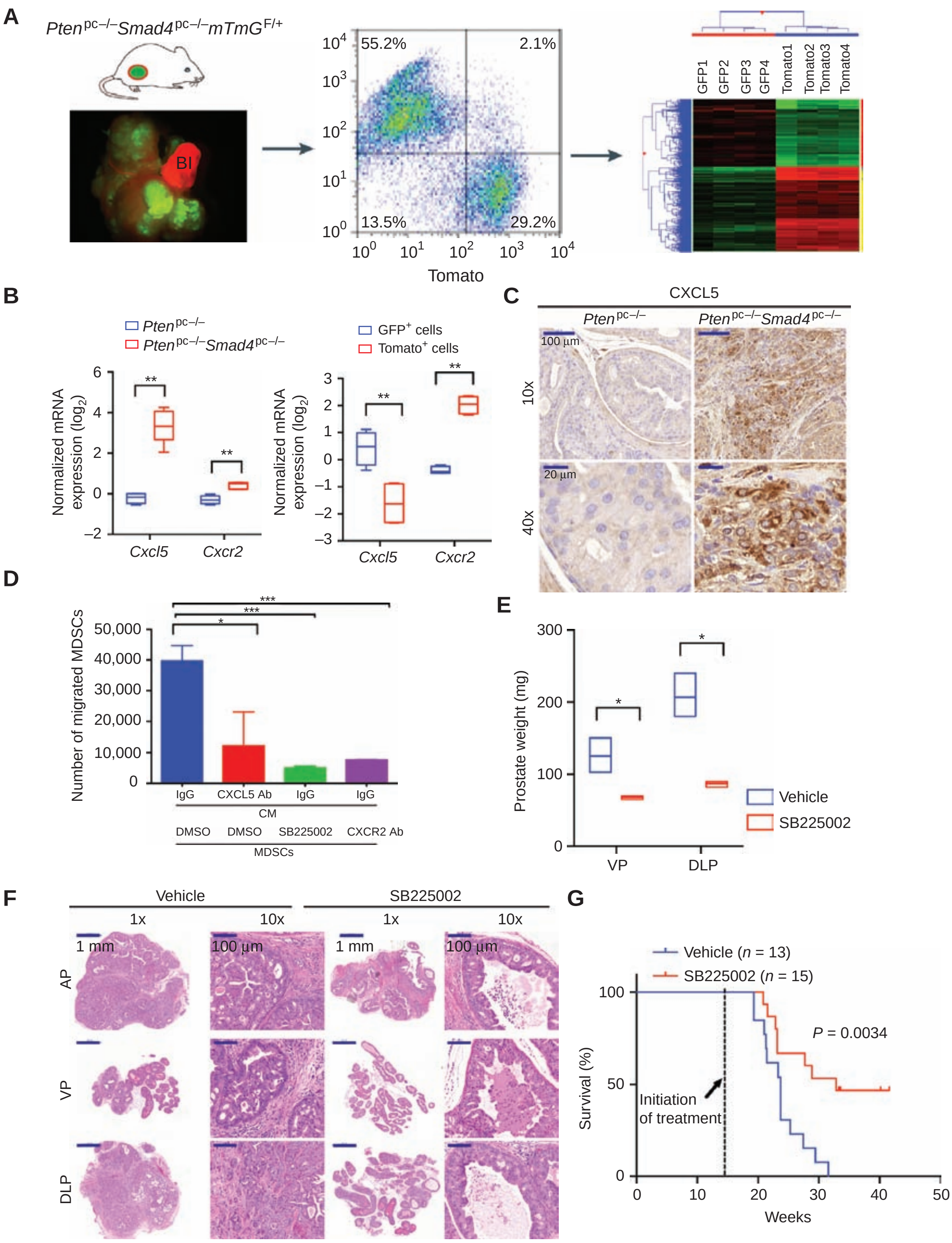

Figure 5. CXCL5–CXCR2 axis plays an indispensable role in recruitment of MDSCs and promotion of tumor progression. **A,** establishment of *Pten*$^{pc-/-}$*Smad4*$^{pc-/-}$*mTmG*$^{+}$ model allows fluorescent visualization of the GFP$^+$ tumor cells intermixed with Tomato$^+$ stroma (left; FACS isolation of GFP$^+$ tumor cells and Tomato$^+$ stromal cells from the prostate adenocarcinoma (middle); microarray analysis to identify differentially expressed genes (right). In the fluorescence image, Bl denotes bladder (completely Tomato$^+$; $n = 2$). **B,** quantification of mRNA expression shows that *Cxcl5* and *Cxcr2* were both expressed at higher levels in *Pten*$^{pc-/-}$*Smad4*$^{pc-/-}$ tumors than in *Pten*$^{pc-/-}$ tumors, and *Cxcl5* expression was enriched in GFP$^+$ tumor cells, whereas *Cxcr2* expression was enriched in Tomato$^+$ stromal cells ($n = 5$). **C,** IHC for CXCL5 showed significantly higher expression levels of CXCL5 in *Pten*$^{pc-/-}$*Smad4*$^{pc-/-}$ tumors than *Pten*$^{pc-/-}$ tumors ($n = 3$). **D,** blocking the CXCL5–CXCR2 axis by CXCL5-neutralizing antibody, CXCR2 inhibitor SB225002, or CXCR2-neutralizing antibody significantly decreased migration of MDSCs toward conditioned medium from *Pten*$^{pc-/-}$*Smad4*$^{pc-/-}$ tumor cells, evaluated with an *in vitro* transwell migration assay in triplicate. **E** and **F,** CXCR2 inhibitor SB225002 treatment of *Pten*$^{pc-/-}$*Smad4*$^{pc-/-}$ mice for 14 days ($n = 4$) resulted in significantly reduced tumor weight of VP and DLP and significantly delayed progression for AP prostate cancer shown by hematoxylin and eosin staining. **G,** CXCR2 inhibitor SB225002 treatment of *Pten*$^{pc-/-}$*Smad4*$^{pc-/-}$ mice significantly prolonged their overall survival. In **B, D,** and **E,** *, $P < 0.05$; **, $P < 0.01$; and ***, $P < 0.001$. Also see Supplementary Fig. S5.

all SB225002-treated tumors presented with prostatic intraepithelial neoplasia (PIN) pathology, whereas the control group uniformly possessed advanced adenocarcinoma (Fig. 5F and Supplementary Table S2). Furthermore, SB225002 treatment significantly prolonged the overall survival of the $Pten^{pc-/-}Smad4^{pc-/-}$ mice as compared with the vehicle control (Fig. 5G). Thus, we conclude that the CXCL5–CXCR2 axis plays a prominent role in the recruitment of MDSCs to the $Pten^{pc-/-}Smad4^{pc-/-}$ prostate TME and that inhibition of this axis profoundly impairs tumor progression.

YAP1 Is Activated in $Pten^{pc-/-}Smad4^{pc-/-}$ Tumors and Directly Regulates *Cxcl5* Transcription

Having identified cancer cell–derived CXCL5 as a key signaling molecule governing recruitment of MDSCs into the TME, we sought to define the molecular mechanisms underlying the strong induction of CXCL5 expression in the $Pten^{pc-/-}Smad4^{pc-/-}$ cancer cells. As CXCL5 expression is not significantly upregulated in the $Pten^{pc-/-}$ tumors (Fig. 5C), we performed unbiased Gene Set Enrichment Analysis (GSEA) to identify pathways that were activated in the $Pten^{pc-/-}Smad4^{pc-/-}$ tumors as compared with $Pten^{pc-/-}$ tumors, aiming to identify potential regulators for *Cxcl5* in $Pten^{pc-/-}Smad4^{pc-/-}$ tumors. The YAP oncogenic signature emerged as the second most hyperactivated pathway (Fig. 6A and Supplementary Fig. S6A). Although it is known that the Hippo–YAP pathway plays an important role in development and cancer in organs such as the liver, skin, intestine, and pancreas (25–27), the role for the Hippo–YAP pathway in prostate cancer biology is emerging. Specifically, Hippo pathway components LATS1/2 have been implicated in anoikis and metastasis in prostate cancer (28), and ERG-induced YAP1 activation can promote age-related prostate tumor development (29). However, beyond the cancer cell–specific functions, the Hippo–YAP1 pathway has not been linked to signaling communication between cancer cells and immune cells in the TME. Consistent with the *in silico* analysis, IHC analysis documented a dramatic increase in the nuclear localization of YAP1 in $Pten^{pc-/-}Smad4^{pc-/-}$ cancer cells as compared with $Pten^{pc-/-}$ cancer cells (Fig. 6B). As YAP1, a transcriptional coactivator and the downstream mediator of Hippo signaling, is regulated posttranscriptionally by either kinase-mediated degradation or cytoplasmic sequestration (25), our findings of increased nuclear localization of YAP1 are consistent with the hypothesis that the Hippo–YAP pathway is activated in the $Pten^{pc-/-}Smad4^{pc-/-}$ tumors. In addition, unbiased oPOSSUM analysis (30) indicated that TEAD1, a member of the TEAD transcription factor family that is required for YAP1 function, ranked second among the top 10 transcription factors with overrepresented binding sites in the 70 cancer-specific genes that were upregulated in the $Pten^{pc-/-}Smad4^{pc-/-}$ tumors as compared with the $Pten^{pc-/-}$ tumors (≥1.5 fold, Z-Score = 13.362; Supplementary Fig. S6B and S6C), an observation reinforcing the relevance of the Hippo–YAP pathway. Furthermore, we identified six YAP/TEAD binding motifs in the promoter of *Cxcl5* gene (Supplementary Fig. S6D), suggesting YAP1 could be directly involved in the recruitment of MDSCs through regulating *Cxcl5* expression. This hypothesis was supported by chromatin immunoprecipitation (ChIP) assay showing that YAP1 binds to *Cxcl5* promoter (Fig. 6C) and that shRNA-mediated knockdown of *Yap1* in $Pten^{pc-/-}Smad4^{pc-/-}$ cancer cells drastically reduced the expression of *Cxcl5* mRNA (Fig. 6D). In addition, overexpression of a constitutively active $YAP1^{S127A}$ mutant dramatically increased *Cxcl5* mRNA expression in the $Pten^{pc-/-}Smad4^{pc-/-}$ cell line (Fig. 6E), whereas overexpression of a TEAD binding defective YAP1 mutant S127A/S94A compromised its ability to activate *Cxcl5* transcription (Fig. 6F). To examine the effect of YAP1-dependent cytokine signaling in the regulation of MDSCs recruitment, we first prepared CM from the $Pten^{pc-/-}Smad4^{pc-/-}$ cell line either infected with shRNA against *Yap1* or pretreated with verteporfin (25), a small-molecular inhibitor that disrupts YAP1–TEAD interaction. We then tested the effect of various CM on the migration of MDSCs *in vitro*. As shown in Fig. 6G and H, we observed significantly decreased MDSC migration *in vitro* when CM was from cells with either YAP1 knockdown or verteporfin treatment.

Finally, to test if targeting YAP1 *in vivo* can impair the infiltration of MDSCs and inhibit tumor growth, we used our recently isolated syngeneic murine prostate cancer line PPS, which is derived from the backcrossed $Pten^{pc-/-}Smad4^{pc-/-}Trp53^{pc-/-}$ model (31) and can form subcutaneous or orthotopic tumors robustly in C57BL/6 hosts. Doxycycline-dependent shRNA knockdown of *Yap1* (two independent shRNA designs #1 and #3) was established in PPS (Fig. 6I) and injected subcutaneously in C57BL/6 mice. YAP1 knockdown induced by switching to doxycycline-containing drinking water resulted in a reduction of MDSCs in the intratumoral $CD45^+$ population (Fig. 6J and K) and impaired tumor progression (Fig. 6L). Although the observation supports the hypothesis that targeting YAP1-dependent MDSC infiltration impairs tumor growth, we acknowledge that the tumor growth impediment by YAP1 silencing is likely due to a combined effect of both cell-nonautonomous and cell-autonomous mechanisms. Together, these findings reveal a novel function for YAP1 in the recruitment of MDSCs through direct upregulation of *Cxcl5* transcription in prostate tumor cells.

YAP1 Is Activated in Human Prostate Cancer and Tracks with an MDSC Signature

To determine whether YAP1 is overexpressed and activated in human prostate cancer, we performed IHC staining of a human prostate cancer tissue microarray (TMA) for YAP1. Interestingly, YAP1 is expressed in basal cells, but not in the luminal cells of the normal human prostate (Fig. 7A). In addition, we observed that YAP1 is overexpressed in a subset of human prostate cancers (Fig. 7A and B and Supplementary Table S6), consistent with a recent report (29). Given the lack of validated antibodies for human MDSCs for TMA analysis, we generated a list of 39 MDSC-related genes curated from literature analysis (Supplementary Table S7) to generate evidence of a link between YAP1 activation and MDSC prominence in human prostate. Using the prostate RNA-sequencing data from The Cancer Genome Atlas (TCGA), unsupervised clustering with the 39-gene MDSC signature categorized 498 TCGA primary prostate tumors into three subtypes: MDSC-high (n = 139), MDSC-medium (n = 158), and MDSC-low (n = 201; Fig. 7C), suggesting that a subset of human prostate tumors may have prominent infiltration of MDSCs. In addition, using GSEA, we found that several YAP1 signature genes are significantly overexpressed in MDSC-high samples as compared with MDSC-low samples (Fig. 7D; P value < 0.005), reinforcing the link between MDSC-high prostate tumors and YAP1 transcriptional activities. Furthermore,

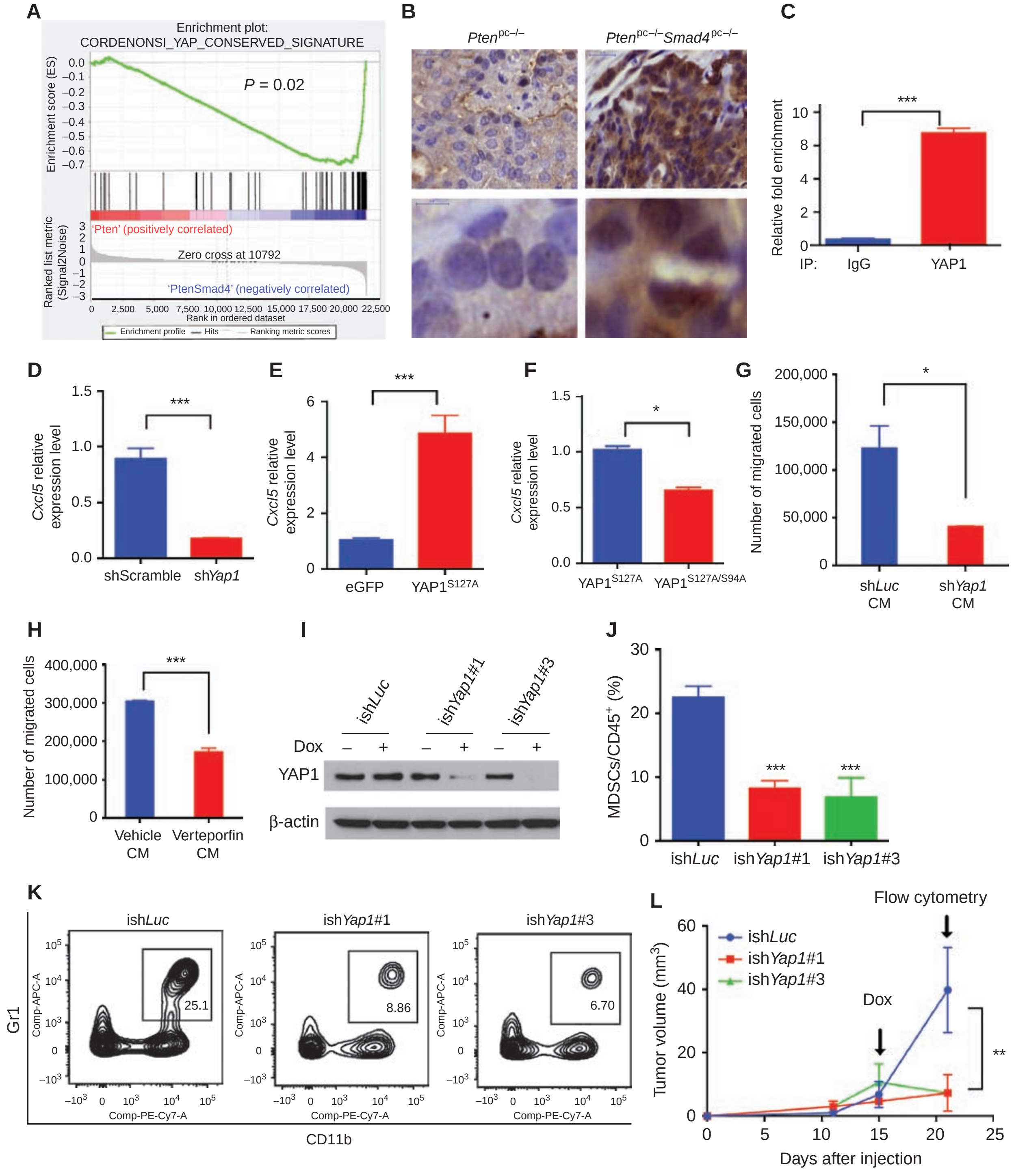

Figure 6. Hyperactivation of YAP1 in *Pten*$^{pc-/-}$*Smad4*$^{pc-/-}$ tumors upregulates *Cxcl5*. **A,** GSEA analysis identified the YAP1 oncogenic signature as the top activated pathway in the *Pten*$^{pc-/-}$*Smad4*$^{pc-/-}$ tumors compared with *Pten*$^{pc-/-}$ tumors ($n = 5$). **B,** a significant increase in nuclear staining of YAP1 in the *Pten*$^{pc-/-}$*Smad4*$^{pc-/-}$ tumors compared with *Pten*$^{pc-/-}$ tumors ($n = 3$). **C,** ChIP shows that YAP1 can directly bind to *Cxcl5* promoter using quantitative PCR in triplicates. **D,** shRNA knockdown of *Yap1* in *Pten*$^{pc-/-}$*Smad4*$^{pc-/-}$ tumor cells resulted in a dramatic reduction in *Cxcl5* mRNA expression using quantitative PCR in triplicate. **E,** overexpression of a constitutively active YAP1^{S127A} mutant resulted in upregulation of *Cxcl5* mRNA using quantitative PCR in triplicate. **F,** TEAD-binding defective YAP1$^{S127A/S94A}$ mutant significantly decreased *Cxcl5* mRNA expression as compared with the YAP1^{S127A} mutant using quantitative PCR in triplicate. **G** and **H,** conditioned medium prepared from *Pten*$^{pc-/-}$*Smad4*$^{pc-/-}$ cells infected with *Yap1* shRNA (**G**) or treated with verteporfin (**H**), a small molecule that disrupts YAP1–TEAD interaction, induced less MDSC migration *in vitro* as compared with the control conditioned medium. Transwell migration was done in triplicate for each condition. **I,** Western blot analysis showed that two independent inducible shRNAs for *Yap1* efficiently knock down *Yap1* expression in the *Pten*$^{pc-/-}$*Smad4*$^{pc-/-}$cells. **J–L,** inducible *Yap1* knockdown strongly suppressed the intratumoral MDSC infiltration (**J** and **K**) and tumor growth (**L**) of the C57BL/6-syngeneic cell line isolated from prostate tumor of *Pten*$^{pc-/-}$*Smad4*$^{pc-/-}$*Trp53*$^{pc-/-}$ mice ($n = 5$). In **C, D, E** and **F, G, H, L,** *, $P < 0.05$; **, $P < 0.01$; ***, $P < 0.001$. See also Supplementary Fig. S6.

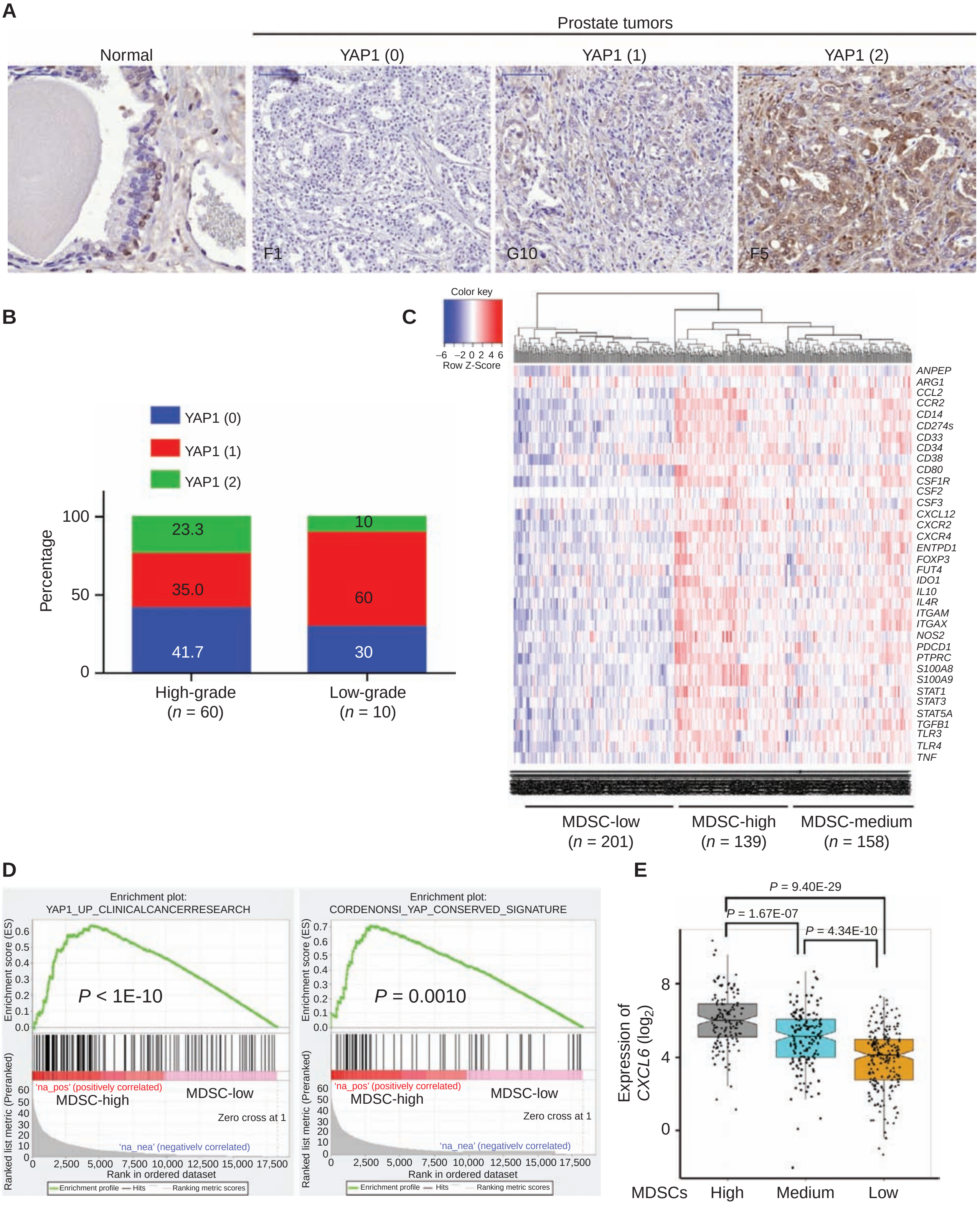

Figure 7. YAP1 is activated in human prostate cancer and correlated with MDSC signature and *CXCL6* overexpression. **A,** IHC analysis of YAP1 expression in basal cells of normal prostate tissue and human prostate cancers. Numbers in parentheses indicate YAP1 IHC intensity scores. **B,** YAP1 IHC intensity score representation in low-grade ($n = 10$) and high-grade ($n = 60$) prostate cancer. **C,** clustering of human TCGA prostate samples into MDSC-high, MDSC-low, and MDSC-medium groups using a 39-gene MDSC signature. **D,** YAP1 signatures are identified in MDSC-high prostate TCGA samples. **E,** *CXCL6* expression is significantly higher in the MDSC-high group. See also Supplementary Fig. S7.

CXCL6, the human homolog of murine *Cxcl5*, is expressed at higher levels in the MDSC-high samples as compared with MDSC-low samples (Fig. 7E; $P = 9.40\text{E}{-}29$). Similar analysis was performed in a published dataset focused on tumor immunobiological differences in prostate cancer between African-American and European-American men (32). The 39-gene MDSC signature can cluster the 69 primary prostate tumors into MDSC-high ($n = 40$) and MDSC-low groups ($n = 29$), and YAP1 signatures were prominent in the MDSC-high groups (Supplementary Fig. S7A and S7B). Together, these human prostate tumor findings, which parallel our murine observations, suggest that activated YAP1 is integral to MDSC infiltration in both mouse and human prostate cancer, thus enhancing the translational value of the study.

DISCUSSION

Although a large number of studies have demonstrated a direct relationship between MDSC frequency and tumor burden (5), our understanding of the role of MDSCs in tumor progression, particularly prostate cancer, remains largely speculative. Here, using a highly invasive PTEN/SMAD4-deficient prostate cancer model, we established the signaling circuits involved in the recruitment of MDSCs to the TME and demonstrated a critical role of these cells in facilitating tumor progression.

Homozygous deletion of *Pten* in murine prostate elicited a strong senescence response that restricts tumor progression (33); thus, *Pten*-deficient prostate tumors are largely indolent and progress slowly to invasive prostate adenocarcinoma without metastasis to distant organs (11, 33). Recently, it was shown that infiltrating Gr1$^+$ myeloid cells suppress *Pten* loss–induced cellular senescence through a paracrine signaling mediated by myeloid-secreted IL1RA (10). We have previously reported that deletion of *Smad4* leads to bypass of *Pten* loss–induced senescence in prostate cancer progression, resulting in aggressive cancer cell proliferation and invasion/metastasis (11). Using the state-of-the-art CyTOF technology, we revealed that progression in the *Pten*$^{pc-/-}$*Smad4*$^{pc-/-}$ model is associated with abundant immune cell infiltration characterized by prominent representation of CD11b$^+$Gr1$^+$ MDSCs, which display potent immunosuppressive activities as shown by their strong antagonistic effect on T-cell proliferation (Fig. 3A and B).

The basis for the increased frequency of MDSCs in the TME and, specifically in the *Pten*$^{pc-/-}$*Smad4*$^{pc-/-}$ model, was not known and presumably could derive from either active chemoattraction or passive nonspecific responses to tissue stress associated with expanding tumor burden. Taking an unbiased approach to identify pathways that may recruit MDSCs, we deconvoluted cancer versus stromal cell transcriptomes by exploiting a Cre-dependent dual fluorescence lineage tracing system in the *Pten*$^{pc-/-}$*Smad4*$^{pc-/-}$ model. This approach identified unique immune regulatory molecules that are activated prominently in *Pten*$^{pc-/-}$*Smad4*$^{pc-/-}$ cancer cells, most prominently CXCL5. We established that the CXCL5 chemokine plays a key role in the efficient recruitment of MDSCs which enables tumor progression, as blocking CXCL5–CXCR2 signaling with a CXCR2 inhibitor led to reduced MDSC infiltration with associated antitumor effects. It should be noted that the human homolog for murine CXCL5 is CXCL6, and CXCL6 has been shown to be upregulated in prostate cancer as compared with normal prostate and significantly associated with high Gleason scores 8 to 9 (34). Interestingly, it was shown that CXCL5 promotes recruitment of MDSCs to primary melanoma, resulting in epithelial–mesenchymal transition (EMT) and cancer cell dissemination (35). Thus, the possible role of CXCL5/CXCL6 in prostate cancer metastasis merits further study.

Our finding that CXCL5 is the main chemoattractant in the *Pten*$^{pc-/-}$*Smad4*$^{pc-/-}$ model also provided a framework to determine the cancer cell signaling pathways driving *Cxcl5* upregulation. By integration of bioinformatic analysis and experimental validation, we identified that YAP1 is activated in *Pten*$^{pc-/-}$*Smad4*$^{pc-/-}$ prostate tumors and that YAP1 directly regulates *Cxcl5* transcription and MDSC recruitment. In addition, we showed that YAP1 is overexpressed in a subset of human prostate cancers, which is consistent with a recent publication showing a correlation of ERG and YAP1 coexpressed in a subset of human prostate cancers (29). Importantly, a 39-gene MDSC signature clusters the prostate TCGA samples into three subtypes. By comparing the samples with high and low abundance of MDSC-related gene expression, YAP1 signatures and higher expression of CXCL6 are identified in the MDSC-high samples, which is consistent with our findings in the mouse model. Furthermore, the 39-gene MDSC signature can cluster primary prostate tumor samples from a published dataset (32) into two subtypes using MDSC-high and MDSC-low, with YAP1 signatures identified in the MDSC-high subtype. The Hippo–YAP signaling pathway is widely deregulated in human solid neoplasia and often associated with enhanced cancer cell proliferation and cancer stem cell phenotypes (25), and is implicated in the regulation of anoikis and metastasis in prostate cancer (28) and the development of age-related prostate cancers driven by ERG overexpression (29), yet how the Hippo–YAP pathway regulates the TME in prostate cancer has hitherto not yet been elucidated. Our finding of a novel non–cell autonomous function for Hippo–YAP signaling in MDSC recruitment in TME complements well the recently elucidated roles of YAP1 in promoting cell-autonomous functionality of cancer cells, including enhanced tumor survival, EMT, and bypass mechanism for oncogene addiction (26, 27).

Pharmacologic depletion of MDSCs using Gr1 antibody, Pep-H6 peptibody, or CXCR2 inhibitor arrested prostate progression at the high-grade PIN stage whereas controls exhibited full-fledged adenocarcinoma in *Pten*$^{pc-/-}$*Smad4*$^{pc-/-}$ model. Given that treatment commences at 14 weeks of age (Supplementary Fig. S3A), when prostate tumors have uniformly advanced to the invasive adenocarcinoma stage (11) with significant MDSC infiltration (Fig. 2B), our findings support the view that anti-MDSC treatment provokes regression of advanced tumors. In addition, both Pep-H6 peptibody and CXCR2 inhibitor treatment significantly prolonged the overall survival of the *Pten*$^{pc-/-}$*Smad4*$^{pc-/-}$ tumor-bearing mice. Therefore, our preclinical data suggest that pharmacologic depletion of MDSCs may offer potential therapeutic benefits for patients with advanced prostate cancer, particularly those deficient for PTEN and SMAD4. In line with our findings, others have demonstrated that depletion of G-MDSCs promotes the intratumoral accumulation of activated CD8$^+$ T cells and apoptosis of tumor epithelial cells in a *Kras/Trp53* mouse pancreatic cancer model (36).

MDSCs are of myeloid cell lineage, and their coordinated regulation represents one of the most complex aspects of cancer–host interactions (37). The involvement of the myeloid compartment of the hematopoietic system in innate immunity, adaptive immunity, as well as in regulation of TME through nonimmune mechanisms highlights the need to understand more deeply how modulating different myeloid populations, including MDSCs, can positively or negatively affect tumor growth.

Pep-H6 peptibody, targeting S100A9 expressed on MDSCs, has been shown to have minimal toxicity in treated mice (20) and potent antitumor activity (Fig. 4D and E; ref. 18). Interestingly, tasquinimod, a small-molecular inhibitor for S100A9, has been shown to increase progression-free survival and overall survival for metastatic castration-resistant prostate cancer in a phase II clinical trial and has entered phase III clinical trials (38). Importantly, similar to the peptibody treatment in mice, tasquinimod is well tolerated and causes only minor adverse effects in human patients (38), suggesting that tasquinimod or similar drugs targeting S100A9 could potentially be used as chemopreventive agents for patients with high-risk primary prostate cancer. The antiproliferative mechanism may explain why targeting CXCR2 in prostate cancer with abundant preexisting MDSC infiltration can lead to MDSC depletion, as MDSCs have been shown to undergo active proliferation inside the prostate tumor of the *Pten*$^{pc-/-}$ model (9). The effectiveness of targeting CXCR2 in our model suggests targeting mechanisms that specifically regulate MDSC recruitment as well as their proliferative and survival potential in human cancers would provide therapeutic benefit for patients with prostate cancer.

Targeting MDSCs as a cooperative approach for immunotherapy is clinically relevant, as increasing evidence indicates MDSCs represent a *bona fide* immunosuppressive cell population in patients with various solid tumors (39, 40). Immunosuppressive mechanisms by MDSCs in mice have been validated in humans, which include L-arginine depletion, NO and ROS production, TGFβ secretion, blocking T_{eff} cells and inducing T_{reg} cells, among others (39). Future studies are warranted to evaluate if combining MDSC depletion with immune checkpoint inhibitors, such as anti–CTLA-4, anti–PD-1, and anti–PD-L1 antibodies, may elicit synergistic efficacy in preclinical models of prostate cancer and eventually benefit patients with prostate cancer.

METHODS

Mice Strains

Pten$^{pc-/-}$ and *Pten*$^{pc-/-}$*Smad4*$^{pc-/-}$ models were developed previously (11) and were backcrossed to the C57BL/6 background for more than four generations. B6.129(Cg)-Gt(ROSA)26Sortm4(ACTB-tdTomato,-EGFP) Luo/J ("mTmG") strain was obtained from The Jackson Laboratory. Mice were maintained in pathogen-free conditions at the MD Anderson Cancer Center. All manipulations were approved under the MD Anderson Cancer Center Institutional Animal Care and Use Committee.

Cell Lines

Pten$^{pc-/-}$*Smad4*$^{pc-/-}$ prostate cell lines, which have been described previously (11), were generated in 2010. PPS, a C57BL/6-syngeneic cell line isolated from prostate tumors of *Pten*$^{pc-/-}$*Smad4*$^{pc-/-}$*Trp53*$^{c-/-}$ mice, was generated in 2013. All cell lines tested for *Mycoplasma* were negative within 6 months of performing the experiments. Cell line authentication was not performed.

CyTOF and Flow Cytometry

Prostate tumor single cells were isolated using the Mouse Tumor Dissociation Kit (Miltenyi Biotec). Single cells were isolated from spleen, lymph node, and peripheral blood using standard protocol. All isolated cells were depleted of erythrocytes by hypotonic lysis. For CyTOF analysis, cells were blocked for FcγR using CD16/CD32 antibody (clone 2.4G2, BD Biosciences) and incubated with CyTOF antibody (DVS Sciences, used at 0.5 test/1 million cells) for 30 minutes at room temperature. Cells were washed once and incubated with MAXPARNucleic Acid Intercalator-^{103}Rh (DVS Sciences) for 20 minutes for viability staining. Cells were fixed with 1.6% formaldehyde for 1 hour and incubated with MAXPARNucleic Acid Intercalator-Ir (DVS Sciences) at 4°C overnight to stain the nuclei. The samples were analyzed with CyTOF instrument (DVS Sciences) in the Flow Cytometry and Cellular Imaging Core Facility at the MD Anderson Cancer Center. Flow cytometry was performed using standard protocol on LSRFortessa analyzer (Becton Dickinson) and analyzed with FlowJo software (Tree Star).

T-cell Suppression and MDSC Migration Assay

T-cell suppression assay was performed as described (9) using FACS-sorted MDSCs and CFSE (Invitrogen)-labeled MACS-sorted (Miltenyi Biotec) CD8$^+$ or CD4$^+$ T cells in anti-CD3– and anti-CD28–coated 96-well plates at an MDSC/T-cell ratio of 0:1, 1:1, 1:2, 1:4, with 3.0×10^5 to 5.0×10^5 MDSCs used in each ratio. Cells were analyzed after 72 hours by flow cytometry, and the suppression of T cells is calculated as described (41). The percentage of CFSE$^+$ cells divided in the presence of MDSCs was compared with the percentage of CFSE$^+$ divided cells in the absence of any added MDSCs. For the MDSC migration assay, an equal number of FACS-sorted MDSCs, untreated or pretreated with neutralizing antibody or inhibitor, were placed on the upper chamber of a transwell system (BD Falcon), and conditioned media from PTEN/SMAD4-deficient cells under various conditions were added to the bottom chamber. Cells were allowed to migrate to the bottom well for 6 hours at 37°C with 5% CO_2. Migrated cells were then analyzed by flow cytometry using BD Fortessa X20. Migrated FITC-positive cells were gated to count the absolute number of cells migrated through the transwell.

MSDC Depletion In Vivo with Gr1 Antibody, Peptibody, and CXCR2 Inhibitor SB225002

Anti-Gr1 (clone RB6-8C5) and isotype control (clone LTF2) were purchased from BioXcell and dosed at 200 μg/mouse (i.p.) every other day. Endotoxin-free plasmids (15 μg) for irrelevant control peptibody (Irr-pep) and MDSC-specific Pep-H6 peptibody were injected into mice through tail vein using the established protocol (21) in TransIT-EE Delivery Solution (Mirus Bio LLC) every 4 days. SB225002 (Cayman Chemical) in DMSO was diluted in vehicle (0.9% NaCl, 0.3% Tween 80) for *in vivo* administration every other day (5 mg/kg).

Inducible Yap1 Knockdown

Inducible *Yap1* knockdown was constructed by cloning the two *Yap1* shRNAs used previously (26) from the pLKO.1 into a doxycycline-inducible plasmid. Lentivirus was packaged in 293T and was used to infect PPS, a C57BL/6-syngeneic cell line isolated from prostate tumor of *Pten*$^{pc-/-}$*Smad4*$^{pc-/-}$*Trp53*$^{c-/-}$mice. Stable sublines were selected with puromycin (2 μg/mL) and injected subcutaneously to the flank of 5-week-old male C57BL/6 mice (Jackson Laboratory). Two weeks after injection, mice were fed with doxycycline water (2 g/L), a method used to execute doxycycline-inducible expression *in vivo* (42). Tumors were measured and extracted 6 days later to analyze for MDSC percentage in infiltrating immune cells.

Computational Analysis of Mouse Microarray Data and Human Prostate TCGA Data

RNA was isolated from FACS-sorted GFP$^+$ and Tomato$^+$ cells using *Pten*$^{pc-/-}$*Smad4*$^{pc-/-}$*mTmG*$^+$ prostate tumors, followed by microarray analysis at the MD Anderson Microarray Core facility using the Mouse Genome 430 2.0 Array (Affymetrix) to generate a *Pten*$^{pc-/-}$*Smad4*$^{pc-/-}$ tumor/stroma dataset GSE71319. Dataset GSE25140 was downloaded from the NCBI Gene Expression Omnibus (GEO) database. Differentially expressed genes between two conditions (GFP$^+$ vs. Tomato$^+$ or PTEN/SMAD4 vs. PTEN) were subjected to IPA, GSEA, and oPOSSUM analysis. For analysis of human prostate data, we first generated a list of 39 human MDSC signature genes by literature mining (Supplementary Table S7). The gene expression data of 498 TCGA prostate samples were downloaded from the Broad GDAC Firehose (http://gdac.broadinstitute.org), which is the RSEM expression estimates normalized to set the upper quartile count at 1,000 for gene level and then with $\log_2$ transformation. The 498 TCGA prostate samples were clustered using the 39 MDSC genes into MDSC-high, MDSC-low, and MDSC-medium (distance between pairs of samples was measured by Manhattan distance, and clustering was then performed using complete-linkage hierarchical clustering). Sixty-nine samples from Wallace and colleagues (32) were clustered into MDSC-high and MDSC-low. Differentially expressed genes between MDSC-high and MDSC-low were analyzed by GSEA. The expression of *CXCL6* in MDSC-high samples is compared with MDSC-low samples using the Wilcoxon test.

Immunohistochemistry and Western Blot Analysis

Tissues were fixed in 10% formalin overnight and embedded in paraffin. IHC was performed as described earlier (11). For Western blot analysis, cells were lysed on ice using RIPA buffer (Boston BioProducts) supplemented with protease and phosphatase inhibitors (Roche). YAP1 antibody was obtained from Novus Bio and Cell Signaling Technology. CXCL5 antibodies were obtained from Bioss and R&D Biosystems. CXCR2 antibody was obtained from Bioss and R&D Biosystems. CD45 and Ly6G antibodies were obtained from Biolegend. Prostate tissue microarray was obtained from Folio Bioscience.

Chromatin Immunoprecipitation

ChIP was performed as described (26) using YAP1 antibody from Novus. Briefly, 5 μg of rabbit IgG (Santa Cruz) or YAP1 antibody was incubated with Protein A Dynabead magnetic beads (Invitrogen) for 4 hours, followed by extensive wash to remove unbound antibody. Antibody beads were then added to the chromatin and incubated overnight. The following primers were used for qPCR analysis: CXCL5_S: 5′-CTCCAGTTTCCTGCCTGAAG-3′ and CXCL5_as: 5′-GTGTGGAG ATTGGGGCTCTA-3′.

Quantitative RT-PCR

RNA was isolated by the RNeasy Kit (Qiagen) and reverse transcribed using the Superscript III cDNA Synthesis Kit (Life Technology). Quantitative PCR was performed using the SYBR-GreenER Kit (Life Technology). The following primers were used: CXCL5_Fwd: GCATTTCTGTTGCTGTTCACGCTG, CXCL5_Rev: CCTCCTTCT GGTTTTTCAGTTTAGC; β-actin_Fwd: GAAATCGTGCGTGACATC AAAG, β-actin_Rev: TGTAGTTTCATGGATGCCACAG; YAP1_Fwd: TGAGATCCCTGATGATGTACCAC, YAP1_Rev: TGTTGTTGTCTGA TCGTTGTGAT.

Statistical Analysis

Data are presented as mean ± SD unless indicated otherwise. The Student *t* test assuming two-tailed distributions was used to calculate statistical significance between groups. Animal survival benefit was determined by the Kaplan–Meier analysis. $P < 0.05$ was considered statistically significant.

Accession Numbers

The expression array data used in this article were in GEO with accession numbers GSE25140 (11) and GSE71319.

Disclosure of Potential Conflicts of Interest

A. Kapoor is a research investigator at Novartis. C.J. Logothetis has received commercial research grants from Astellas, BMS, J&J, Excelixis, Pfizer, Novartis, Bayer, AstraZeneca, and Helsinn HC. No potential conflicts of interest were disclosed by the other authors.

Authors' Contributions

Conception and design: G. Wang, X. Lu, Z. Ding, C.J. Logothetis, Y.A. Wang, R.A. DePinho
Development of methodology: G. Wang, X. Lu, P. Dey, P. Deng, V. Ramamoorthy, Q. Chang
Acquisition of data (provided animals, acquired and managed patients, provided facilities, etc.): G. Wang, X. Lu, P. Dey, P. Deng, Z. Fang, S. Hua, E.M. Li-Ning-Tapia, Z. Guo, X. Shang, S. Khadka, E.-J. Jin, X. Pan, L. Li, Q. Chang, P. Troncoso, M.J. McArthur
Analysis and interpretation of data (e.g., statistical analysis, biostatistics, computational analysis): G. Wang, X. Lu, P. Dey, C.C. Wu, J. Zhang, C.-J. Wu, N.B. Patel, Y. Shi, Q. Chang, C.J. Logothetis, M.J. McArthur, Y.A. Wang
Writing, review, and/or revision of the manuscript: G. Wang, X. Lu, P. Dey, C.C. Wu, C.-J. Wu, C.J. Logothetis, M.J. McArthur, Y.A. Wang, R.A. DePinho
Administrative, technical, or material support (i.e., reporting or organizing data, constructing databases): P. Dey, P. Deng, C.C. Wu, S. Jiang, R. Konaparthi, E.M. Li-Ning-Tapia, A. Kapoor, N.B. Patel, Z. Guo, T. Heffernan, D. Zhao, X. Shang, P. Hou, B. Hu, W. Yao, Y. Shi, L. Chin
Study supervision: Y.A. Wang, R.A. DePinho
Other (mouse work): K. Zhao
Other (assessed immunohistochemical stains): E.M. Li-Ning-Tapia
Other (supported molecular biology needs, i.e., cloning): T.N. Tieu

Acknowledgments

The authors thank Drs. Larry W Kwak and Hong Qin for the peptibody plasmids; Drs. Willem Overwijk and Yared Hailemichael for advice in hydrodynamic injection; Samirkumar Amin and members of the DePinho laboratory for helpful suggestions and technical support; and the Flow Cytometry and Cellular Imaging Core Facility (Jared Burks, Duncan Mak, and Karen Dwyer) and the Sequencing & Non-coding RNA Core Services (Chang-Gong Liu) at The University of Texas MD Anderson Cancer Center (Cancer Center Support Grant CA16672).

Grant Support

The project was supported by U01CA141508 (to L. Chin and R.A. DePinho), Prostate Cancer Research Program (PCRP) W81XWH-13-1-0202 (to G. Wang) and W81XWH-14-1-0429 (to P. Dey); the Idea Development Award–New Investigator Option (W81XWH-14-1-0576; to X. Lu) from the Department of Defense; and the Clayton & Modesta Williams Cancer Research Fund. Additional support was provided by the Jane Coffin Childs Memorial Fund Postdoctoral Fellowship to X. Lu. E.-J. Jin is supported by Korean Governments (MISP) grant number 2011-0030130.

Received February 23, 2015; revised October 5, 2015; accepted October 16, 2015; published OnlineFirst December 21, 2015.

REFERENCES

1. Karlou M, Tzelepi V, Efstathiou E. Therapeutic targeting of the prostate cancer microenvironment. Nat Rev Urol 2010;7:494–509.
2. Junttila MR, de Sauvage FJ. Influence of tumour micro-environment heterogeneity on therapeutic response. Nature 2013;501:346–54.
3. Hanahan D, Coussens L. Accessories to the crime: functions of cells recruited to the tumor microenvironment. Cancer Cell 2012;21: 309–22.
4. Hanahan D, Weinberg Robert A. Hallmarks of cancer: the next generation. Cell 2011;144:646–74.
5. Talmadge JE, Gabrilovich DI. History of myeloid-derived suppressor cells. Nat Rev Cancer 2013;13:739–52.
6. Vuk-Pavlović S, Bulur PA, Lin Y, Qin R, Szumlanski CL, Zhao X, et al. Immunosuppressive CD14+HLA-DRlow/− monocytes in prostate cancer. Prostate 2010;70:443–55.
7. Idorn M, Kollgaard T, Kongsted P, Sengelov L, Thor Straten P. Correlation between frequencies of blood monocytic myeloid-derived suppressor cells, regulatory T cells and negative prognostic markers in patients with castration-resistant metastatic prostate cancer. Cancer Immunol Immunother 2014;63:1177–87.
8. Brusa D, Simone M, Gontero P, Spadi R, Racca P, Micari J, et al. Circulating immunosuppressive cells of prostate cancer patients before and after radical prostatectomy: profile comparison. Int J Urol 2013;20:971–8.
9. Garcia AJ, Ruscetti M, Arenzana TL, Tran LM, Bianci-Frias D, Sybert E, et al. Pten null prostate epithelium promotes localized myeloid-derived suppressor cell expansion and immune suppression during tumor initiation and progression. Mol Cell Biol 2014;34:2017–28.
10. Di Mitri D, Toso A, Chen JJ, Sarti M, Pinton S, Jost TR, et al. Tumour-infiltrating Gr-1+ myeloid cells antagonize senescence in cancer. Nature 2014;515:134–7.
11. Ding Z, Wu CJ, Chu GC, Xiao Y, Ho D, Zhang J, et al. SMAD4-dependent barrier constrains prostate cancer growth and metastatic progression. Nature 2011;470:269–73.
12. Bjornson ZB, Nolan GP, Fantl WJ. Single-cell mass cytometry for analysis of immune system functional states. Curr Opin Immunol 2013;25:484–94.
13. Youn JI, Nagaraj S, Collazo M, Gabrilovich DI. Subsets of myeloid-derived suppressor cells in tumor-bearing mice. J Immunol 2008;181:5791–802.
14. Kusmartsev S, Nefedova Y, Yoder D, Gabrilovich DI. Antigen-specific inhibition of CD8+ T cell response by immature myeloid cells in cancer is mediated by reactive oxygen species. J Immunol 2004;172:989–99.
15. Szuster-Ciesielska A, Hryciuk-Umer E, Stepulak A, Kupisz K, Kandefer-Szerszen M. Reactive oxygen species production by blood neutrophils of patients with laryngeal carcinoma and antioxidative enzyme activity in their blood. Acta Oncol 2004;43:252–8.
16. Schmielau J, Finn OJ. Activated granulocytes and granulocyte-derived hydrogen peroxide are the underlying mechanism of suppression of T-cell function in advanced cancer patients. Cancer Res 2001;61:4756–60.
17. Pekarek LA, Starr BA, Toledano AY, Schreiber H. Inhibition of tumor growth by elimination of granulocytes. J Exp Med 1995;181:435–40.
18. Wang G, Lunardi A, Zhang J, Chen Z, Ala U, Webster KA, et al. Zbtb7a suppresses prostate cancer through repression of a Sox9-dependent pathway for cellular senescence bypass and tumor invasion. Nat Genet 2013;45:739–46.
19. Lunardi A, Ala U, Epping MT, Salmena L, Clohessy JG, Webster KA, et al. A co-clinical approach identifies mechanisms and potential therapies for androgen deprivation resistance in prostate cancer. Nat Genet 2013;45:747–55.
20. Qin H, Lerman B, Sakamaki I, Wei G, Cha SC, Rao SS, et al. Generation of a new therapeutic peptide that depletes myeloid-derived suppressor cells in tumor-bearing mice. Nat Med 2014;20:676–81.
21. Liu F, Song Y, Liu D. Hydrodynamics-based transfection in animals by systemic administration of plasmid DNA. Gene Ther 1999;6: 1258–66.
22. Muzumdar MD, Tasic B, Miyamichi K, Li L, Luo L. A global double-fluorescent Cre reporter mouse. Genesis 2007;45:593–605.
23. Yang L, Huang J, Ren X, Gorska AE, Chytil A, Aakre M, et al. Abrogation of TGF beta signaling in mammary carcinomas recruits Gr-1+CD11b+ myeloid cells that promote metastasis. Cancer Cell 2008;13:23–35.
24. Bierie B, Stover DG, Abel TW, Chytil A, Gorska AE, Aakre M, et al. Transforming growth factor-beta regulates mammary carcinoma cell survival and interaction with the adjacent microenvironment. Cancer Res 2008;68:1809–19.
25. Johnson R, Halder G. The two faces of Hippo: targeting the Hippo pathway for regenerative medicine and cancer treatment. Nat Rev Drug Discov 2014;13:63–79.
26. Kapoor A, Yao W, Ying H, Hua S, Liewen A, Wang Q, et al. Yap1 activation enables bypass of oncogenic Kras addiction in pancreatic cancer. Cell 2014;158:185–97.
27. Shao DD, Xue W, Krall EB, Bhutkar A, Piccioni F, Wang X, et al. KRAS and YAP1 converge to regulate EMT and tumor survival. Cell 2014;158:171–84.
28. Zhao B, Li L, Wang L, Wang CY, Yu J, Guan KL. Cell detachment activates the Hippo pathway via cytoskeleton reorganization to induce anoikis. Genes Dev 2012;26:54–68.
29. Nguyen LT, Tretiakova MS, Silvis MR, Lucas J, Klezovitch O, Coleman I, et al. ERG activates the YAP1 transcriptional program and induces the development of age-related prostate tumors. Cancer Cell 2015;27:797–808.
30. Kwon AT, Arenillas DJ, Worsley Hunt R, Wasserman WW. oPOSSUM-3: advanced analysis of regulatory motif over-representation across genes or ChIP-Seq datasets. G3 2012;2:987–1002.
31. Ding Z, Wu C-J, Jaskelioff M, Ivanova E, Kost-Alimova M, Protopopov A, et al. Telomerase reactivation following telomere dysfunction yields murine prostate tumors with bone metastases. Cell 2012;148:896–907.
32. Wallace TA, Prueitt RL, Yi M, Howe TM, Gillespie JW, Yfantis HG, et al. Tumor immunobiological differences in prostate cancer between African-American and European-American men. Cancer Res 2008;68:927–36.
33. Chen Z, Trotman LC, Shaffer D, Lin HK, Dotan ZA, Niki M, et al. Crucial role of p53-dependent cellular senescence in suppression of Pten-deficient tumorigenesis. Nature 2005;436:725–30.
34. Liu Q, Russell MR, Shahriari K, Jernigan DL, Lioni MI, Garcia FU, et al. Interleukin-1beta promotes skeletal colonization and progression of metastatic prostate cancer cells with neuroendocrine features. Cancer Res 2013;73:3297–305.
35. Toh B, Wang X, Keeble J, Sim WJ, Khoo K, Wong WC, et al. Mesenchymal transition and dissemination of cancer cells is driven by myeloid-derived suppressor cells infiltrating the primary tumor. PLoS Biol 2011;9:e1001162.
36. Stromnes IM, Brockenbrough JS, Izeradjene K, Carlson MA, Cuevas C, Simmons RM, et al. Targeted depletion of an MDSC subset unmasks pancreatic ductal adenocarcinoma to adaptive immunity. Gut 2014;63:1769–81.
37. Gabrilovich DI, Ostrand-Rosenberg S, Bronte V. Coordinated regulation of myeloid cells by tumours. Nat Rev Immunol 2012;12:253–68.
38. Osanto S, van Poppel H, Burggraaf J. Tasquinimod: a novel drug in advanced prostate cancer. Future Oncol 2013;9:1271–81.
39. Filipazzi P, Huber V, Rivoltini L. Phenotype, function and clinical implications of myeloid-derived suppressor cells in cancer patients. Cancer Immunol Immunother 2012;61:255–63.
40. Solito S, Marigo I, Pinton L, Damuzzo V, Mandruzzato S, Bronte V. Myeloid-derived suppressor cell heterogeneity in human cancers. Ann N Y Acad Sci 2014;1319:47–65.
41. Battaglia M, Stabilini A, Roncarolo MG. Rapamycin selectively expands CD4+CD25+FoxP3+ regulatory T cells. Blood 2005;105:4743–8.
42. Ying H, Kimmelman AC, Lyssiotis CA, Hua S, Chu GC, Fletcher-Sananikone E, et al. Oncogenic Kras maintains pancreatic tumors through regulation of anabolic glucose metabolism. Cell 2012;149: 656–70.